CHALMERS
UNIVERSITY OF TECHNOLOGY

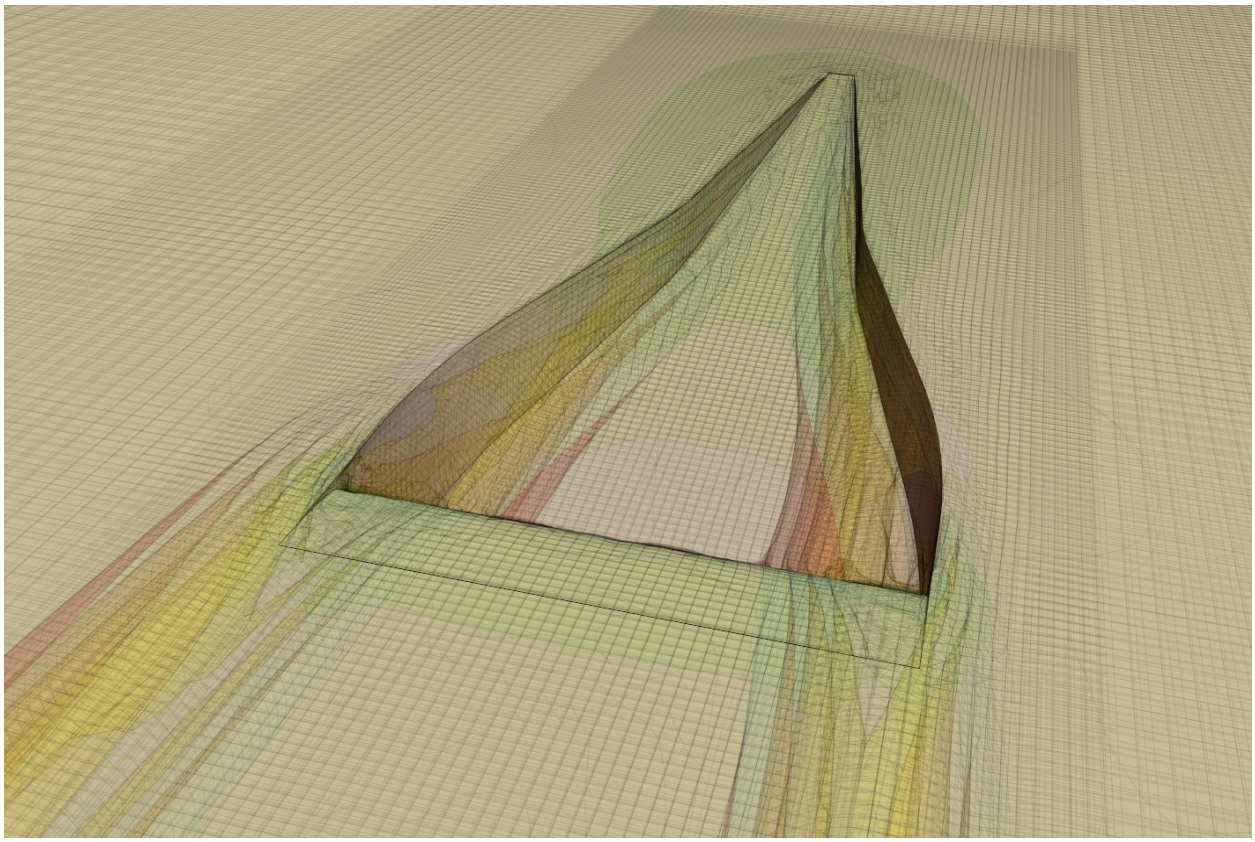

NACA Ducts in vehicle thermal simulations

An investigation of steady state CFD methods for modelling cooling flows through submerged inlets

Master's thesis in MPAME

ABHILASH MENON

Department of Applied Mechanics
CHALMERS UNIVERSITY OF TECHNOLOGY
Gothenburg, Sweden 2017

Master's thesis 2017:60

NACA Ducts in vehicle thermal simulations

An investigation of steady state CFD methods for modelling cooling flows through submerged inlets

ABHILASH MENON

CHALMERS
UNIVERSITY OF TECHNOLOGY

Department of Applied Mechanics
Division of Fluid dynamics
Chalmers University of Technology
Gothenburg, Sweden 2017

NACA Ducts in vehicle thermal simulations
An investigation of steady state CFD methods for modelling cooling flows through submerged inlets
ABHILASH MENON

Supervisors: Niklas Löfgren and Athanasios Tzanakis, Volvo Cars Corporation
Examiner: Lars Davidson, Department of Applied Mechanics

Master's Thesis 2017:60
Department of Applied Mechanics
Division of Fluid Dynamics
Chalmers University of Technology
SE-412 96 Gothenburg
Telephone +46 31 772 1000

Cover: Total pressure iso-surfaces showing the formation of vortex sheets along the walls of a NACA duct

Typeset in LaTeX
Gothenburg, Sweden 2017

NACA ducts in vehicle thermal simulations
An investigation of steady state CFD methods for modelling cooling flows through submerged inlets
ABHILASH MENON
Department of Applied Mechnics
Chalmers University of Technology

Abstract

NACA ducts are a class of low-drag submerged inlets that find use in aircraft for cooling flows and as engine intakes. Due to their aesthetic appearance and design flexibility, car makers sometimes opt to use NACA ducts for similar applications, especially for high performance vehicles. They are most commonly found on the bonnet or on the side panels. This study concerns NACA ducts located on the under-body of cars, the purpose of which are to provide cooling flows for critical components in the engine bay. The objective was to develop a steady steady state CFD model which can capture the inducted cooling flow and also to assess if this model can be integrated into a "full-car" thermal simulation.

A preliminary study was conducted using experimental data, available in literature, for NACA ducts. The information obtained from this was used to simulate under-body ducts on a production car inside a reduced domain which contained parts of the engine bay. Due to the lack of experimental data for the under body ducts, the steady state method was tested against a *Large eddy simulation* of the reduced domain using identical boundary conditions.

The results of the study reveal that a steady state approach can accurately estimate the flow rate through the ducts. The flow immediately downstream of the duct is also captured. However, it's not accurate enough for the complex flows inside the engine bay, away from the ducts. The study concludes that it would be ill advised to integrate this into a full car simulation as even a slight change in the cooling flow path might lead to erroneous results.

Keywords: NACA Ducts, cooling flows, vehicle thermal simulation, CFD, LES, RANS.

Acknowledgements

The study presented in this report was performed at Volvo Cars Corporation, Sweden, from January to June 2017. I thank them for taking me in and for providing this wonderful opportunity. A special thanks to my supervisors Niklas Löfgren and Athansios Tzanakis for sharing their expertise and invaluable guidance. I would like to thank Lars Davidson, professor at Chalmers Institute of Technology, for accepting this work and acting as the examiner. Lastly, I thank my friends, family and colleagues for their continuing support.

Abhilash Menon, Gothenburg, June 2017

Contents

List of Figures

List of Tables

1
Introduction

1.1 Background

During the 1940's the National Advisory Committee for Aeronautics (NACA), precursor to modern day NASA, designed and tested a series of submerged inlets. The objective was to investigate the potential of low drag inlet designs for use in jet engines. This was part of the early attempts at supersonic flight. Submerged inlets of this type became known colloquially as *NACA ducts* or *NACA inlets*. After extensive testing and implementation in a few aircraft, notably in the North American YF93 series as shown in Figure 1.1, submerged designs saw little use in jet aircraft as engine inlets due to their inherent limitations. The design could not generate the high mass flows necessary for a jet engine, as compared to more conventional inlets such as scoops. They did, however, possess characteristics that suited them for piston engine inlets as well as cooling flow applications.

Figure 1.1: North American YF93A used by NACA as a test platform for submerged inlets

Due to their shape, NACA ducts exhibit reduced form drag as compared to annular inlets and also have a reduced tendency to induce flow separation[1]. This, combined with greater flexibility in terms of location, make submerged inlets an attractive option for aerodynamic cooling in automobiles[4]. Submerged inlets have been suc-

cessfully used in high performance vehicles for cooling flows as well as engine inlets. When used, they are usually located on the bonnet or side panels; regions usually associated with thin boundary layers and positive pressure gradients. Increasingly, they're finding use in everyday cars.

Figure 1.2: NACA duct on a high performance car

This study concerns the cooling flow through NACA ducts locate on a car underbody. More specifically, the ducts that are integrated into the engine under shield designed to cool some critical components in the engine bay.

Figure 1.3: Engine under shield with integrated NACA ducts

The study was carried out at Volvo Cars Corporation, Gothenburg. It uses one of their production models as a test bed to study computational methods for simulating the flow through the above mentioned ducts. *Computational Fluid dynamics* (CFD) tools available were used for this purpose.

1.2 Motivation

Thermal regulation is an important aspect of vehicle design. Engineers make great efforts to ensure that components can reliably handle operating temperatures and that overheating is prevented by adopting suitable cooling strategies. In this regard, thermal simulation using CFD is widely used by car makers during the design phase to check component reliability, cooling performances and to spot potential design flaws. It is not unusual to simulate the entire car with many of its internal and external flows in a vehicle thermal simulation. This may include flows through coolant pipes, cooling fans and heat exchangers.

In the context of this study, it is beneficial to have a CFD method that can adequately handle cooling flows through under-body NACA ducts. This would enable engineers to simulate duct operation and the effect of their sizing, shape and location. It would also be beneficial if this can be integrated into a full vehicle thermal simulation to check if the target components are being cooled enough.

The research on NACA ducts in ground vehicle applications has been scarce[4]. Also, there is little published work on duct induced cooling flows in vehicle engine bays. Furthermore, it is extremely difficult to perform experimental flow visualization in the engine bay due to space constraints and highly turbulent flows.

1.3 Problem description

The CFD method currently used in vehicle thermal simulation does not fully describe the flow through under-body NACA ducts. It is a steady state method and current simulations show that one of the NACA ducts on the selected car is non functional, while tests in the wind tunnel show that it works satisfactorily for the same driving case. This makes it difficult to trust the simulations and calls for a more suitable method that can capture these cooling flows for different driving cases. Additionally, flow fields inside the engine bay can be rather complex because of the irregular geometries of numerous components that share a limited space. This makes experimental flow visualization rather difficult. Considering this, accurate simulations may be the only convenient way to estimate cooling flow paths for the under-body ducts.

1.4 Project aims and research questions

The goal of this thesis is to produce a steady state CFD method which can handle cooling flows through under-body NACA ducts. It employs the *Reynolds-averaged Navier-Stokes (RANS)* equations and involves developing a meshing strategy along with suitable choice of a turbulence model. It is pertinent to investigate the following questions.

1. How accurately can the method model the flow patterns and known performance characteristics of a NACA duct?

2. Is it able to capture the complex flow patterns inside the engine bay? This would greatly affect usability.
3. Can it be integrated into a full vehicle thermal simulation? And if not, how else can it be made useful?

1.5 Scope and limitations

It cannot be claimed that the method described here is generalized to all types of ground vehicles as it was developed using a single car geometry. The car used here is the 2018 year model Volvo XC60. Due to time constraints, under-body ducts were simulated at a single free stream velocity in the "head-on" condition i.e. there are no cross-winds lateral to the car's orientation.

1.6 Approach Summary

The design guidelines and experimental data regarding submerged inlets published by NACA are available in the public domain. Design guidelines in [1] were used to replicate a generic NACA duct geometry as a CFD model. This was used in a preliminary study to develop a RANS method to capture flow behaviour under different operating conditions. Several numerical studies were referenced during method development. For example, [2] used *Detached Eddy Simulation* to model the aerodynamic and aero-acoustic properties of a NACA duct geometry identical to the one used for the preliminary study.

The RANS method developed during the preliminary study is then used to simulate under-body ducts on the car. However, there was still the issue of not having a reference case for this, needed to validate the RANS method. A *Large Eddy simulation* (LES) was performed for a reduced domain which contained three of the five NACA ducts on the car geometry. Boundary conditions for the reduced domain were extracted from an existing simulation, this ensured a semi-realistic description of the inducted flow as well as flow in the engine bay. The LES was the "best possible" simulation that could have been performed given the time, skill and resource restrictions.

The results from the LES are then used as a reference to validate the RANS model. For an accurate evaluation, the RANS method is also developed for the same reduced test domain and for identical boundary conditions. All simulations were performed on STAR-CCM+ (Version 11.04.012) and CFD models constructed using ANSA (Version 17.0.1).

1.7 Thesis outline

The proceeding parts of the thesis are structured as follows:

1. Chapter 2 "Theory": Information about NACA ducts with regards to their construction and associated flow behaviour, definitions of performance variables, key concepts used for the CFD modelling, key concepts used for the LES model.
2. Chapter 3 "Methods": Details the simulations and post processing techniques used during method development.
3. Chapter 4 "Results and discussion": Enlists key findings
4. Chapter 5 "Conclusion": Evaluation and assessment of the method

2

Theory

2.1 Construction and working of NACA ducts

Submerged inlets consists of a sloping ramp flanked by walls. Theses walls can be parallel, divergent or convergent (Figure 2.1). NACA duct configurations usually have curved diverging walls and usually also have a lip with a curved profile, shown in Figure 2.2. The main design variables that determine the shape of a NACA duct are the width-depth ratio, the ramp floor angle, curvature of the lip and the plan-form of the divergent walls. The NACA ducts on the car under-body have a similar shape except for the lip profile.

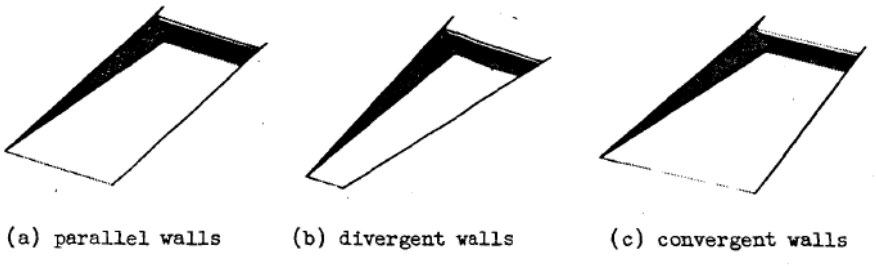

Figure 2.1: Three classes of submerged inlets. Figure from reference [3]

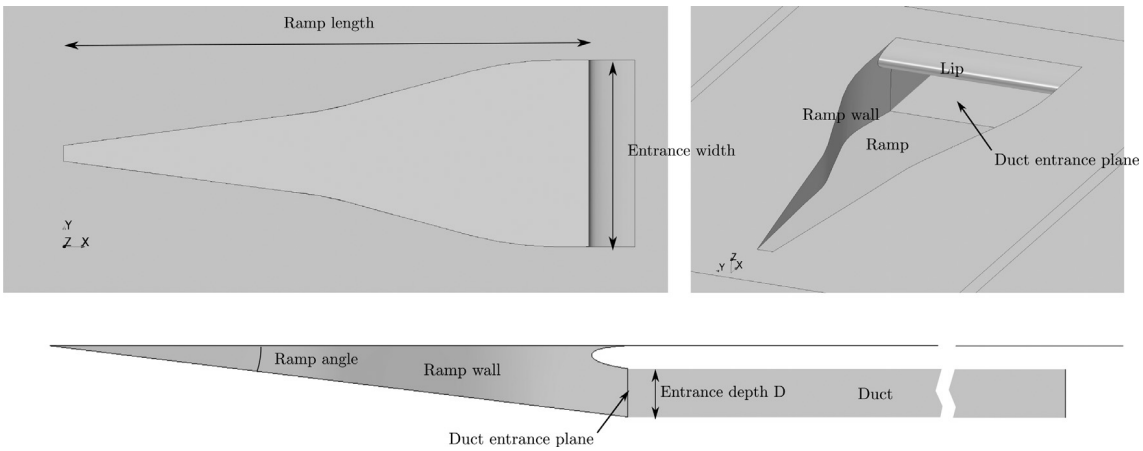

Figure 2.2: Construction of a NACA duct with curved divergent walls. Figure from reference [2]

2.1.1 Flow behaviour

The flow over a submerged inlet with divergent walls is three dimensional and can be complex even at low speeds. The external flow is not parallel to the walls and will tend to spill over the edges. If the velocity over the corner is to remain finite, a vortex sheet must develop along the edge of the divergent walls, shown in Figure 2.3 from [3]. It is theorized that these vortex sheets interact with the boundary layers formed over the ramp and floor, effectively whisking them away from the duct entrance. This prevents the slow moving air from entering the duct and thus reduces the inlet losses[3]. The boundary layer along the floor covers a larger wetted area than that on the walls and has more of an effect on the duct performance. The boundary layer growth here depends on the pressure distribution which is determined the inlet geometry and operating conditions[3]. The performance of a NACA duct is sensitive to upstream boundary layer profiles as well as the incidence (yaw) angle[4].

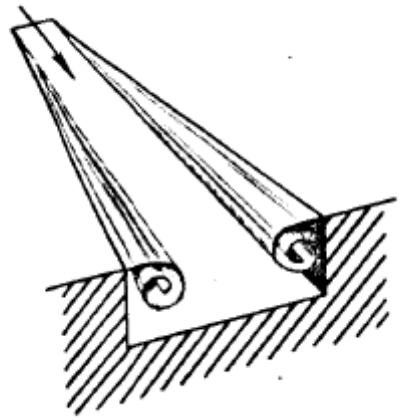

Figure 2.3: Vortex sheet forming along the edge of diverging walls. Figure from reference [3]

The slope of the ramp floor and the plan-form of the divergent walls are kept gentle to prevent boundary layer separation, which will adversely affect the inlet performance. The optimal inlet design was found to have width-depth ratio of 4 and a ramp angle of 7° [2]. This geometry is replicated for the first half of this study. The design details are given in Appendix A.

2.1.2 Experimental setup

Figure 2.4 shows part of the experimental setup used by NACA for measuring inlet performance at different operating conditions. Rakes consisting of total pressure and static pressure tubes were located at the duct inlet to measure pressure recovery (see 2.2.2). Static pressure distribution over the ramp and the lip were obtained using flush orifices and pressure tubes. The rectangular cross section of the inlet leads to a circular duct through a diffuser section. A centrifugal blower at the end of the

duct is used to obtain a range of velocity ratios (see 2.2.1), flow control is obtained by means of a venturimeter located in the duct[1].

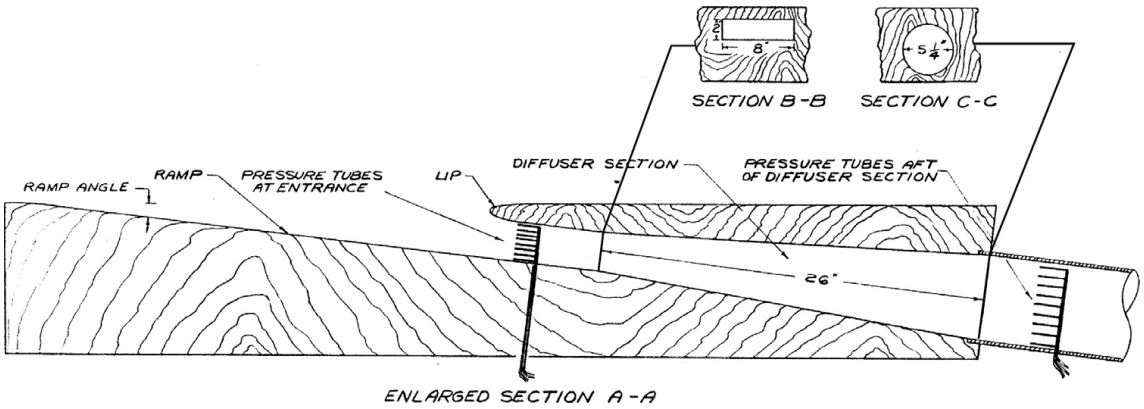

Figure 2.4: Experimental setup used by NACA to test duct performance. Figure from reference [1]

2.2 Non-dimentional parameters

Several non-dimensional parameters are used to gauge inlet performance at different operating conditions. These were used during method validation. The definitions are obtained from [1].

2.2.1 Inlet velocity ratio

Inlet velocity ratio, ν, is defined as the ratio of average velocity at duct entrance to the axial free stream velocity.

$$\nu = \frac{V_1}{V_0} \tag{2.1}$$

Index 0 represents the free stream while 1 represents quantities averaged over the duct entrance plane.

2.2.2 Ram recovery ratio

Used by NACA researchers to gauge the inlet performance for different geometries and different velocity ratios.

$$\rho = \frac{P_{T,1} - p_0}{P_{T,0} - p_0} \tag{2.2}$$

where P_T is total pressure and p is static pressure

2.2.3 Pressure coefficient

Pressure coefficient is used to show flow behaviour over the ramp as well as the lip.

$$C_p = \frac{p - p_0}{\frac{1}{2}\rho_0 V_0^2} \tag{2.3}$$

where ρ represents density.

2.3 CFD simulation

Steady state CFD simulations were used for the selected NACA duct geometry as well as under-body ducts on the car using the RANS solver in STAR-CCM+. All the simulations were three dimensional assuming adiabatic surfaces. This is true for the LES as well.

2.3.1 Mesh generation

STAR-CCM+ uses the finite volume method for which the flow domain needs to be divided into small discrete volumes. The automated mesh option in STAR-CCM+ was used for all simulations performed for this thesis. The *trimmed cell mesher* creates a structured mesh primarily consisting of hexaherdal elements with minimal cell skewness along with ploy hedral trimmed cells near the surfaces. The cells can be aligned as to a specified coordinate system and volumetric controls can be used for refining the mesh in specific regions for increased accuracy. A structured mesh has lesser memory requirements than an unstructured mesh of comparable size, generally allowing for faster computation.

Aligned meshes of this type are prone to numerical dissipation in regions where the flow direction is diagonal to the elements. This is a source of error that needs to be minimized. Figure 2.5 from [6] illustrates this problem. It shows a flow domain having uniform inviscid flow where the fluid in the top half is "painted" with a passive scalar of 0 while the bottom half is painted with 1. The fluid moves from left to right. Clearly, there is diffusion of the passive scalar when the mesh is not aligned to the flow.

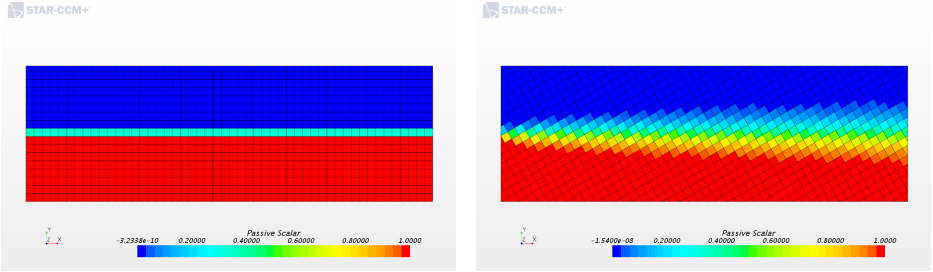

(a) Trimmed mesh aligned with the flow

(b) Trimmed mesh aligned diagonal to the flow

Figure 2.5: Numerical dissipation for a trimmed cell mesh. Figures from reference [6]

The polyhedral mesher in STAR-CCM+ generates an unstructured mesh. Polyhedral cells typically have 14 faces[5]. Volumetric controls can be used for local mesh refinement, as before. Numerical dissipation can be reduced by refining the mesh, see Figure 2.6 from [6], this could improve the solution accuracy when complex flow patterns are involved. Both polyhedral and trimmed mesh types were used during the study for their inherent advantages.

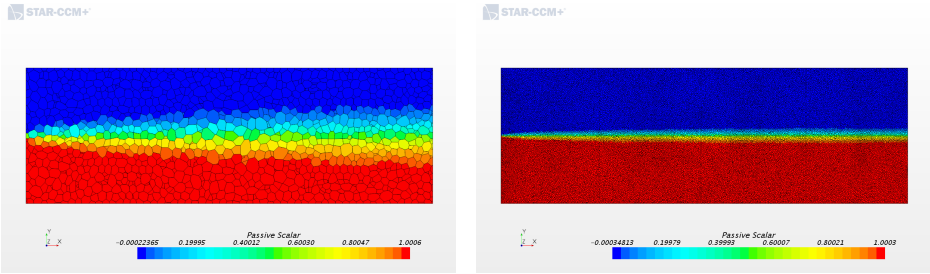

(a) Ployhedral mesh used for an identical case

(b) Improved solution using a more refined mesh

Figure 2.6: Numerical dissipation for a polyhedral mesh. Figures from reference [6]

2.3.2 Boundary layer resolution

In order to improve the accuracy of the solution, it is required to adequately resolve the boundary layer and the high normal velocity gradients near the wall. This is important when flow features like separation are involved, which in turn affect the local pressure drop. The viscous sub-layer in turbulent boundary flow can be resolved using prism layers, if the selected turbulence model supports a high fidelity mesh near the wall. A coarser mesh would require the code to employ wall functions, which is less accurate but is more efficient computationally. Prism layers allow for high aspect ratio cells which can increase the mesh density in the cross stream direction while keeping the cell count low. It also reduces numerical dissipation near the walls thus improving accuracy[5]. The number, size and growth of the prism cells in the wall normal direction are designed prior to mesh generation for a targeted value of *wall y+* (see 2.3.4).

2.3.3 Turbulence modelling

The turbulent stress term in the RANS equation is approximated using mathematical models in CFD, when direct resolution of turbulent structures is not practical. The choice of model greatly affects the accuracy of the solution. Some of the parameters to be considered when selecting a model are stability, boundary layer treatment and performance under certain flow conditions. As mentioned before, the performance of a NACA duct is sensitive to the upstream boundary layer, this necessitates a turbulence model that would support a high mesh fidelity near the wall. The $k-\epsilon$ and $k-\omega$ turbulence models are two equation "eddy-viscosity based" models that are commonly used in CFD when using the RANS method. The $k-\omega$ model is

know to perform better for boundary layer flows in adverse pressure gradients while $k-\epsilon$ is less sensitive to free stream conditions[5]. The $k-\omega$ SST model effectively combines $k-\omega$ in the near wall region with $k-\epsilon$ away from the wall using a blending function thereby reducing the sensitivity issue for the standard $k-\omega$ model. The more complex *Reynold's Stress Transport* model performs better the eddy-viscosity models when the flow is strongly curved or undergoes strong rotations. However, it can be quite unstable[5].

2.3.4 Wall y+

The *wall y+* is a normalized wall distance. It may be used as a reference to determine center of the first cells near a wall. Some turbulence models allow for a low value of y+ (≈ 1) i.e. a high mesh fidelity near the wall and a more accurate simulation. If the first cells near a wall correspond to a high y+ value (≈ 30), the turbulence model may resort to wall functions to approximate near wall effects.

$$y^+ = \frac{yu^*}{\nu} \tag{2.4}$$

In Equation 2.4, y is the normal distance from the wall , ν is the turbulent viscosity, and u^* is a reference velocity defined as

$$u^* = \sqrt{\tau_w/\rho} \tag{2.5}$$

where τ_w is the wall shear stress. In CFD codes, however, u^* is defined in quantities specific to the selected turbulence model. When designing a mesh it is sometimes desirable to calcuate the grid spacing near the surface for a targeted value of y^+. The following equations are taken from reference [7].

$$Re_x = \rho U_\infty L\mu \tag{2.6}$$

$$C_f = \frac{0.026}{Re_x^{\frac{1}{7}}} \tag{2.7}$$

Equation 2.6 gives the Reynolds number near a flat plate a distance L from the edge while 2.7 gives the value of skin friction coefficient C_f for turbulent flat plate boundary layer flow. C_f is defined as

$$C_f = \frac{\tau_w}{0.5\rho U_\infty^2} \tag{2.8}$$

which gives

$$\tau_w = \frac{C_f \rho U_\infty^2}{2} \tag{2.9}$$

this allows for calculating u^* using Equation 2.5. Subsequently, using 2.4 gives us

$$y = y^+ \nu u^* \tag{2.10}$$

which can be used as a reference to locate the centers of the near wall cells. For LES the stream-wise ($x+$) and span-wise ($z+$) quantities are also critical and are defined in a similar way. The recommendations for LES are that the $y+$ be less than 1 and also $x+ < 100$ and $z+ < 30$ for the near wall cells[9].

2.4 Large eddy simulation

Large eddy simulation is a class of time-dependent (unsteady) simulation where the large scale turbulent structures are resolved by the mesh and the smaller scales are modelled by so called *sub-grid models*. Since most of the turbulence is being explicitly solved for, the error in turbulence modelling has a less of an impact on the solution accuracy. The best results can be obtained using *Direct Numerical Simulation* (DNS) where all the scales are resolved. However, this is extremely expensive computationally and is not practical for most CFD applications.

2.4.1 Sub-grid scale models

Unlike the RANS equations, the LES equations are obtained through a process of spacial filtering, as opposed to time averaging. The term analogous to the turbulent stress term in the RANS equation is known as the *sub-grid stress*. It needs to be modelled and represents the small scale eddies. Sub-grid scale models approximate the sub-grid stress tensor. The models available were the *Smagorinsky*, *Dynamic Smagorinsky*, and *Wall-adapting Local Eddy-Viscosity* (WALE) models. WALE is known to be less sensitive than the other two due to a its internal setup and performs well near walls[5].

2.4.2 Temporal schemes

Implicit and explicit solution methods are available for the LES. Although implicit schemes are more computationally demanding, requiring several inner iterations per time step, they afford us the use of larger time steps and greater stability. This could potentially reduce the LES solution time, where an explicit scheme would require an impractically small time step for stability. Additionally, 1^{st} or 2^{nd} order temporal discretization may be used, where 2^{nd} order schemes offer greater accuracy but can be unstable.

2.4.3 Approximating dissipative scale lengths

Knowledge of the range of sizes for the smallest turbulent structures in the flow domain may be helpful in designing the mesh for an LES. The Kolmogorov length scale is the size of the smallest, dissipative, eddies in the flow domain and is defined as [9]

$$\lambda_\eta = \left(\frac{\nu_t^3}{\epsilon}\right)^{(1/4)} \tag{2.11}$$

where ν_t is the turbulent viscosity and ϵ is the dissipation rate. Full car simulations referenced for the study used the $k-\epsilon$ turbulence model. Kolmogorov length scales can be approximated using

$$\lambda_\eta = C_\mu^{3/4}\frac{k^{3/2}}{\epsilon} \tag{2.12}$$

since $\nu = C_\mu(k^2/\epsilon)$ for $k-\epsilon$ turbulence[9]. k is the turbulent kinetic energy and C_μ is a model constant.

2.4.4 Quality checks for the LES

The following concepts were used when performing the LES to check its quality. They reveal if the mesh and time resolution are adequate for a good simulation.

2.4.4.1 Convective Courant number

The Convective Courant number is a the ratio of the physical time step to the convection time scale for the mesh. For a 1 dimensional case it is defined as

$$C = \frac{u\Delta t}{\Delta x} \leq C_{Max} \tag{2.13}$$

where u is the velocity magnitude, Δt is the time step and Δx is the interval length. Equation 2.13 is known as the *Courant-Friedrichs-Lewy* condition and is a necessary stability condition for the numerical solution of time-dependent partial differential equations[8]. A Courant number of 1 or less ensures that a fluid 'particle' will not traverse a distance more that the dimensions of a cell during one time step, this could potentially increase the solution accuracy.

2.4.4.2 Resolved and modelled turbulent kinetic energy

As mentioned before, an LES aims to resolve most of the turbulent structures while modelling the smallest scales which are to expensive to resolve. The following scalar is used to approximate the LES quality in the domain

$$M = \frac{k_{SGS}}{k_{res} + k_{SGS}} \tag{2.14}$$

where k_{SGS} is the modelled turbulent kinetic energy obtained from the sub-grid scale model. K_{res} is the turbulent kinetic energy resolved by the mesh and is defined as[9]

$$K_{res} = \langle(\tilde{u}_i - \langle\tilde{u}_i\rangle_T)(\tilde{u}_i - \langle\tilde{u}_i\rangle_T\rangle_T \tag{2.15}$$

where $\tilde{u}_i$ is the instantaneous velocity in i and $\langle\rangle_T$ represents time averaging. The ratio of turbulent kinetic energy to the sub-grid kinetic energy above 5 ($M \leq 0.2$) in the region of interest is acceptable for LES[5].

3
Methods

3.1 Preliminary study on a generic NACA duct

The goal of the preliminary study was to produce a RANS method which can model the flow behaviour of a generic NACA duct. The method is validated using experimental data in literature.

3.1.1 CFD model and simulation domain

The design guidelines in [1] were used to replicate a NACA duct geometry as a CFD model. It has a flat 7° ramp, curved divergent walls and a width-depth ratio of 4, as shown Figure 3.1. The design details are provided in Appendix A.

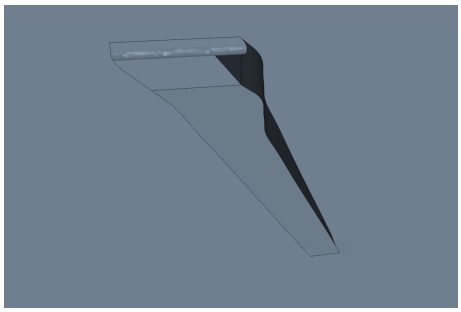

Figure 3.1: CFD model geometry for a generic NACA duct

An identical geometry is studied in [2] for its aero-acoustic properties using *Detached Eddy Simulation*, which is a combination of RANS and LES. This study was used a reference for creating the flow domain, shown in Figure 3.2. The domain consists of a velocity inlet, pressure outlet and a mass flow outlet. The top wall and side walls are symmetry planes while the floor, inlet surface and duct are represented as no-slip walls. The setup allows for the control of the free stream velocity above the duct surface. All simulations were performed for a free stream velocity of 60 m/s, consistent with the available experimental data for the geometry. The NACA inlet opens into a rectangular duct section which extends about $1m$ into a mass flow outlet. This is different from the experimental setup in [1] in which the NACA duct opens into a circular diffuser. The diffuser section is not modelled here but should not be an appreciable source of error as measurements were taken upstream of the diffuser[2]. The addition of a mass flow outlet allows for the control of the axial velocity inside the duct and thus controlling the velocity ratio, defined in 2.2.1.

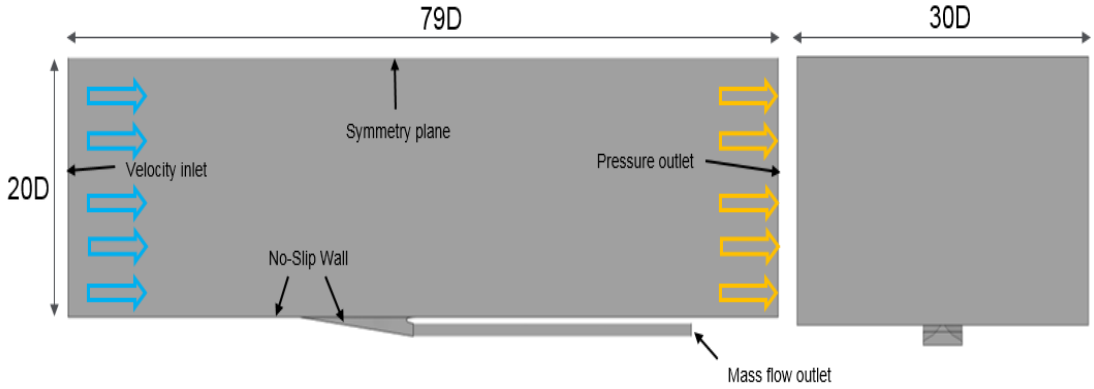

Figure 3.2: CFD domain used for preliminary study. D = Duct Entrance depth (Left) Profile; (Right) Front view

Since the NACA duct is sensitive to upstream boundary layer conditions, it is imperative that the boundary layer profile in the CFD simulations and the wind tunnel match closely. The boundary layer profile for the wind tunnel was measured where the tip of the duct would be located, this is shown in Figure 3.3. A steady state simulation was run in a domain identical to Figure 3.2, except without the NACA duct, and velocity profiles were measured at different distances from the inlet (also in Figure 3.3) to find the location where the boundary layer profile approximately matches that of the wind tunnel. The duct tip is then located here for all CFD simulations in the preliminary study (1.25 m from the velocity inlet).

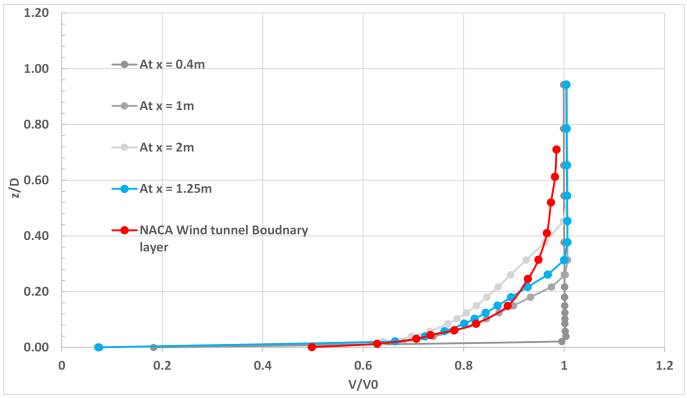

Figure 3.3: Boundary layer profile for the NACA wind tunnel and CFD simulation. Experimental data from reference [1].

3.1.2 Mesh design

The domain in Figure 3.2 is meshed using the trimmed cell mesher in STAR-CCM+. The trimmed cell option was chosen since it would be easier to integrate this method for the under-body ducts into a full car simulation. The mesh needs to be able to capture the vortex sheet formation, discussed in 2.1.1, to represent the behaviour of a NACA duct. Volumetric refinement was performed near the inlet geometry using concentric cylindrical refinement zones, see Figure 3.4. The isotropic cell size is

controlled relative to the base size for the trimmed cell mesher. From the outermost refinement zone to the innermost, the relative size is reduced as 50%, 25% and 12.5% of the base size respectively. This progressive decrease maintains a high mesh quality.

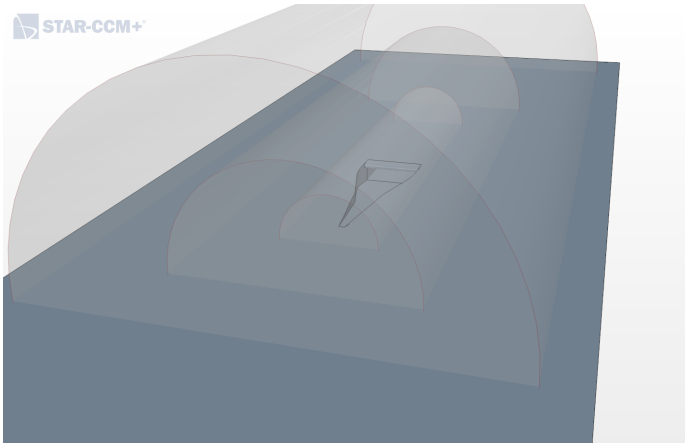

Figure 3.4: Mesh refinement zones, relative sizes and locations.

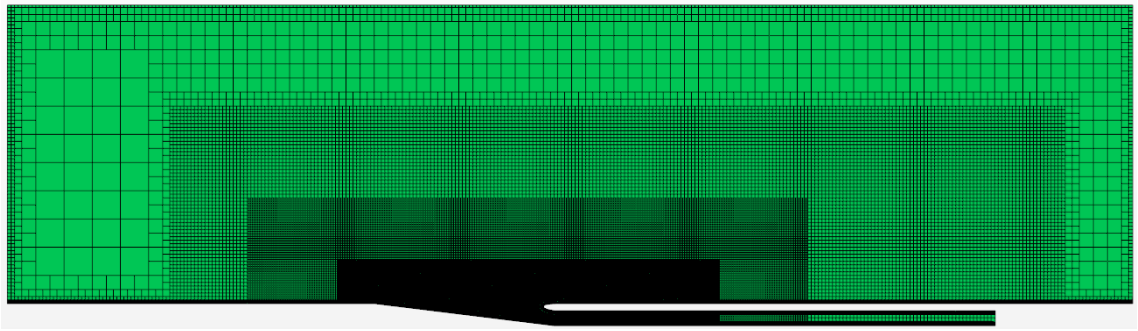

Figure 3.5: Mesh design for the preliminary study, profile view.

Configuration	Zone diameters			Zone lengths			Distance from duct tip		
	d_1/D	d_2/D	d_3/D	l_1/D	l_2/D	l_3/D	t_1/D	t_2/D	t_3/D
1	23.63	11.82	5.91	54.23	32.45	17.73	12.80	8.55	2.53
2	25.60	13.79	5.91	54.23	37.41	25.60	12.80	8.55	2.53

Table 3.1: Refinement zone sizes and location. D = Duct entrance depth

Mesh	Configuration	Base Size (mm)
0.49M cells	2	100
1.8M cells	1	60
2.6M cells	2	60
4.1M cells	2	50
5.9M cells	1	40
7.2M cells	2	40

Table 3.2: Base sizes for different meshes

The boundary layer is resolved using prism cells. The height of the boundary layer is approximated to be the height above the wind tunnel floor at which the air velocity (axial to the inlet) reaches 99% of its free stream value. From [1], this is approximately $13mm$. A total of 18 prism layers were used having a growth ratio of 1.3. This was chosen as it should give a *wall y+* value of 3 (see 2.3.4).

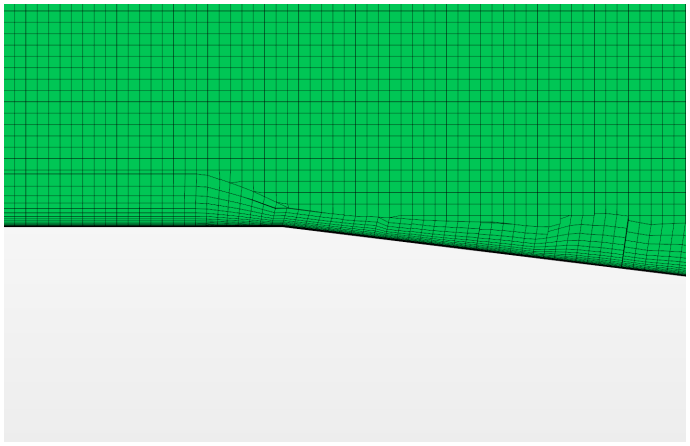

(a) Mesh near the tip of the NACA duct.

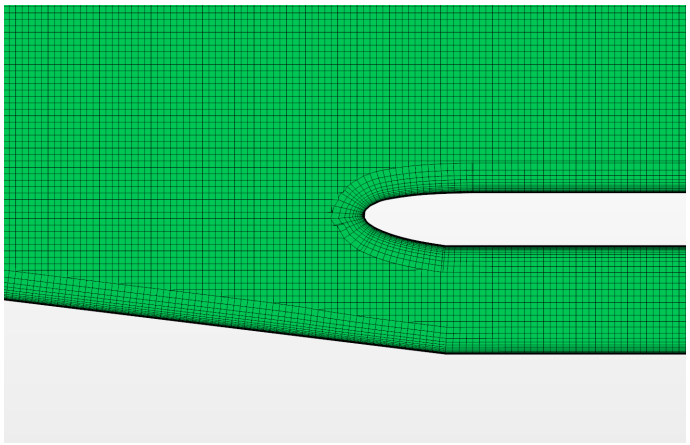

(b) Mesh near the entrance plane and lip.

Figure 3.6: Mesh design for preliminary study, close-up view.

3.1.3 Case setup and physics models

Steady state simulations for the preliminary study were setup using the constant density gas model in STAR-CCM+. The in-built *Air* model was used for the domain with standard density and viscosity values. It is reasonable to assume incompressible flow for the sub-sonic conditions that were simulated. $k-\omega$ SST turbulence model was selected for the RANS solver for its accurate performance for boundary layer flows in adverse pressure gradients which are expected near the diverging walls of the NACA duct.

3.1.4 Boundary conditions, initialization and convergence

The velocity inlet generates a constant normal velocity of 60 m/s across its surface while the pressure outlet maintains a static pressure of 1 atm. This provides the required free stream velocity. The velocity ratio (ν) is controlled by adjusting the mass flow through the duct outlet. Assuming constant density, the mass flow is calculated as:

$$\dot{m} = \nu \rho A V_0 \tag{3.1}$$

where ρ is the fluid density, A is the area of the duct outlet and V_0 the free stream velocity. The solver then calculates the back pressure that should be applied to maintain the mass flow through the duct outlet, this is done for every iteration. The simulations were initialized using the *Grid Sequencing* expert algorithm in STAR-CCM+ which computes an approximate inviscid solution for the flow variables. This was done to reduce the solution time. To assess simulation convergence, the axial velocity and static pressure averaged over the duct entrance plane were monitored along with points in the wake region.

3.1.5 Preliminary study findings summarized

The results of the preliminary study are discussed in Section 4.1. The study provided information useful for developing a method for the under-body ducts. Hence, the findings are summarized here.

1. A steady state RANS method using a simple mesh refinement strategy and a suitable turbulence model can adequately simulate NACA duct behaviour over a range of operating conditions. The velocity ratios thought to be interesting for under-body ducts ($0.6 < \nu < 1.0$) show good results.
2. Complex interactions between the boundary layer and vortex sheets may not be fully captured but it should still give good estimates for the flow through the duct.
3. It may not give accurate results in a small range of velocity ratios where the duct is operating around its "transition" region ($0.3 < \nu < 0.5$). The range of this region depends on the geometry and is difficult to guess for each duct.

3.2 Test domain for under-body NACA ducts

In order to develop a CFD method for the under-body NACA ducts, a test domain was constructed using the geometry of a production model car. The selected car has five under-body ducts integrated into the engine under-shield. The domain is essentially a "box" which contains three of these ducts, a section of the car under-side, some components in the engine bay and a surface which represents the road. Figures 3.7 and 3.8 show how the domain is located.

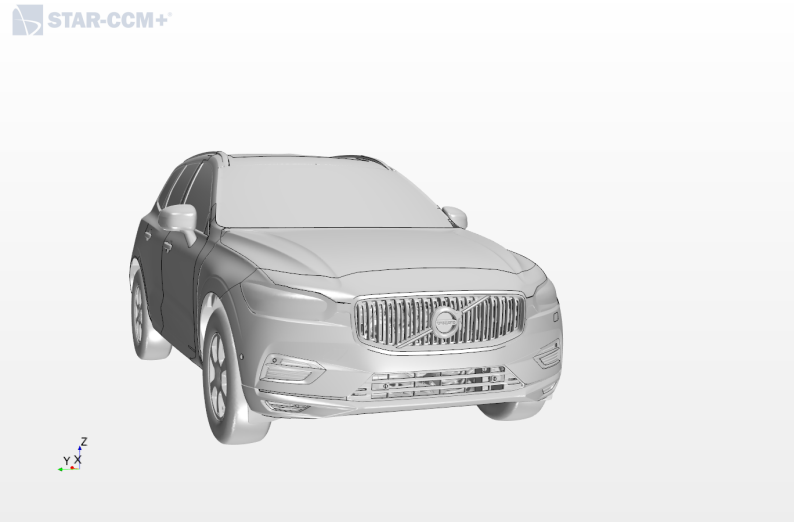

(a) Selected car geometry (Volvo XC60).

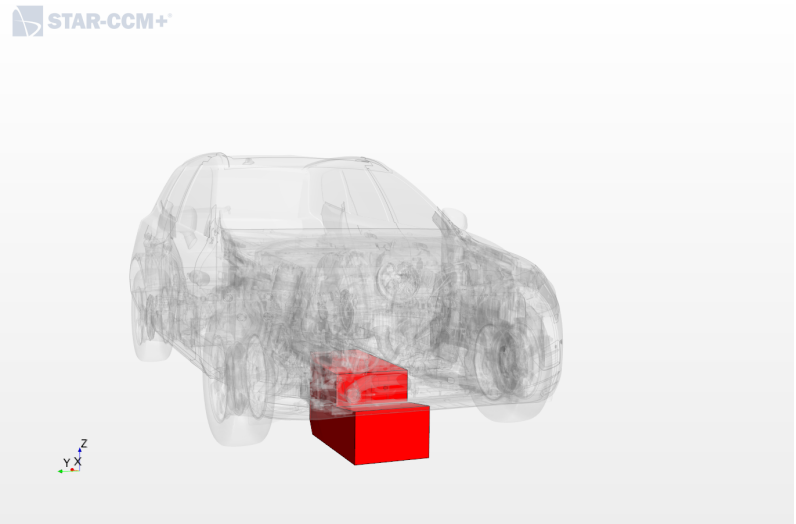

(b) Relative position of the test domain.

Figure 3.7: Test domain for under-body ducts.

The shape and size of the "box" was decided based on the following.

1. It should cover as much of the car under-side as possible upstream of the duct for the boundary layer to develop.

2. The cooling fan is avoided for simplicity. Inclusion of this would require modelling the moving blades of the fan. This would make the model unnecessarily complex.
3. The size of the domain is kept modest to reduce computational costs.

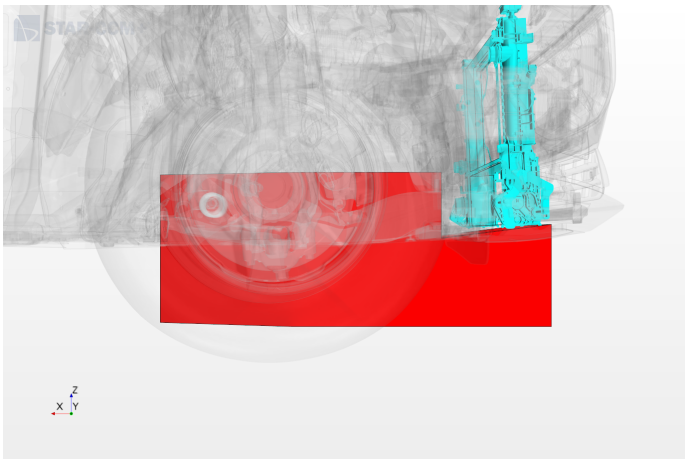

Figure 3.8: Test domain viewed in profile, the cooling pack frame is highlighted in blue.

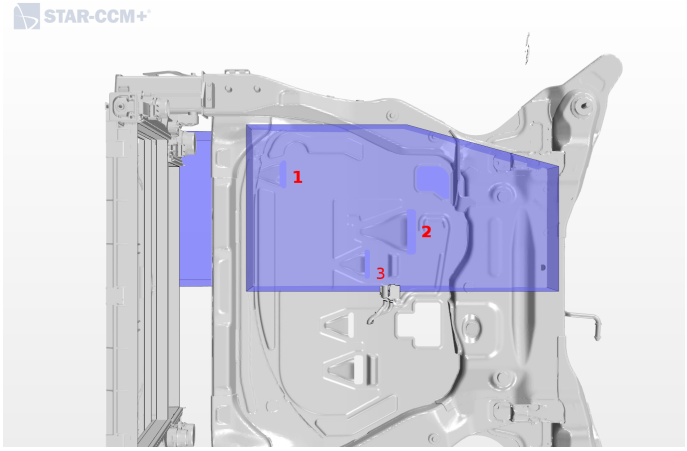

Figure 3.9: Test domain relative to the engine under-shield and sub-frame, as viewed from the top; Contains three under-body ducts (numbered 1-3).

The *surface wrapper* tool in STAR-CCM+ was used to generate the surface mesh for the test domain. This creates a closed "water-tight" domain that is confined by the domain box. Figure 3.10 shows that the geometry of the flow domain that lies inside the engine bay is rather complex. The quality of the surface mesh is high since it was generated directly from the geometry CAD data for the components. Additionally, the mesh resolution was kept fine with a base size of 2 mm for the triangular elements that represent the surfaces. The target size was 100% of the base size and minimum size as 10% of the base size.

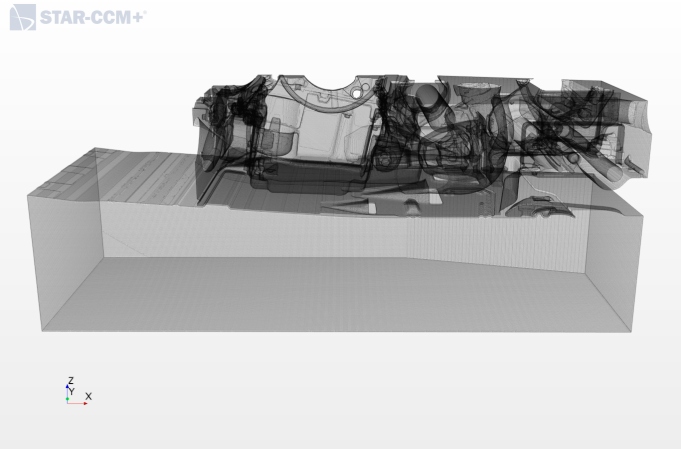

Figure 3.10: Surface mesh for the test domain geometry.

3.3 Reference case using LES

There is no available experimental data which can be used to visualize the flow fields inside bay and cooling flows through the NACA ducts. It was decided that a "best possible" simulation performed on the test domain using realistic boundary conditions will serve as a reference used for validating the steady state model. Of the CFD methods that were available for this study, LES had the highest accuracy and was selected for generating the reference case.

3.3.1 Mesh for the LES

A high quality, high resolution mesh is required to obtain good results for LES. Polyhedral mesh was chosen for this purpose as it is less prone to numerical dissipation for complex flow fields. To get an idea of the cells sizes that would be required, the existing CFD model using $k - \epsilon$ turbulence was taken and dissipative scale-lengths were approximated (Equation 2.12) using point probes in the region of interest (inside the test domain). Table 3.3 shows that a fine mesh resolution is required inside the engine bay and near the under-body but a coarser mesh will do for the flow outside the car. The external flow field is not of much interest for this study and coarsening the mesh here is desired as it would decrease the cell count.

Point	Location	λ_η mm
1	Near the engine under-shield	0.89
2	Inside the engine bay	5.07
3		2.92
4		1.93
5		1.44
6	Free stream below the under-body	8.98

Table 3.3: Approximate dissipative scale lengths for the existing full car simulation.

The base size of 1.5 mm was selected for the polyhedral mesh inside the car and 20 mm in the free-stream. Prism cells were used to resolve the boundary layer. The mesh was designed to give a low $y+$ value near the walls ($y^+ \approx 1$) and the prism cell growth rate limited to 1.1. The stream-wise and span-wise quantities are approximated as $x+ = z+ \approx 8.32$ near the engine under-shield. A total of 52 layers were used based on the required near-wall grid spacing (see 2.3.4) as well as to prevent an abrupt increase in cell size between the prism layers and the bulk mesh. The resulting mesh has around 77 million cells.

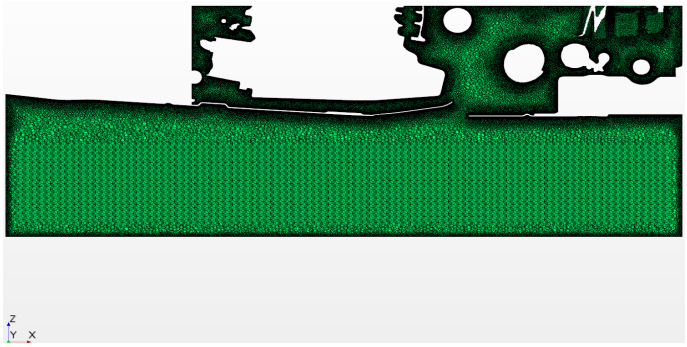

Figure 3.11: Polyhedral mesh for the LES, section view through mid-plane of Duct 2

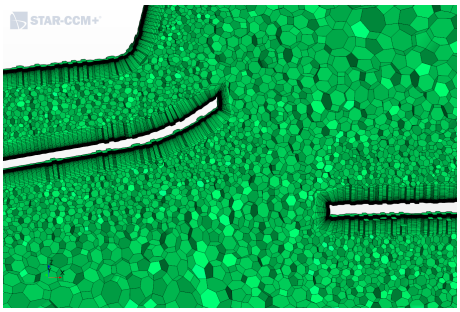

(a) Section view, profile, duct mid-plane.

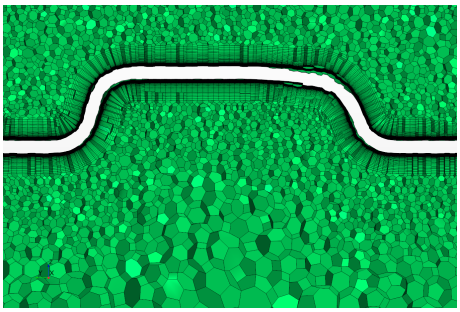

(b) Section view, front, duct entrance plane.

Figure 3.12: Mesh for LES around Duct 2

3.3.2 Boundary conditions for the test domain

The boundary conditions for the test domain were mapped from the existing full-car simulation which was setup for a driving speed of 70 kph ($\approx 19.44\ m/s$). The front and top sides of the domain box was designated as velocity inlets while the rear side as pressure outlets. This should give a realistic description of flow conditions.

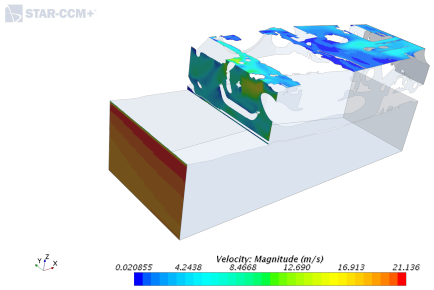

(a) Velocity inlet, mapped velocity components v_x, v_y and v_z

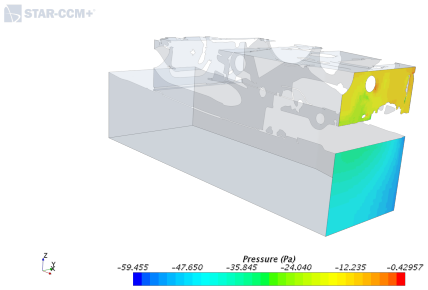

(b) Pressure outlet, mapped static pressure p

Figure 3.13: Boundary conditions for the test domain.

The sides of the box are symmetry planes. This was done in order to prevent over-constraining the LES which could lead to divergence issues and also risk the LES solution conforming too much with the steady state model. The road surface is modelled using a moving no-slip wall where the tangential velocity is set to represent a driving speed of 70 kph.

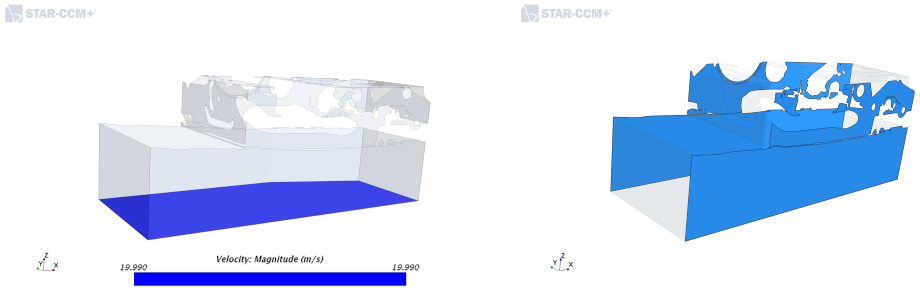

(a) Moving no-slip wall, $v_x = 20\ m/s$

(b) Symmetry planes

Figure 3.14: Boundary conditions for the test domain.

3.3.3 Simulation setup

The LES simulation was initialized from a converged RANS solution which used $k-\omega$ SST turbulence. This was done to reduce the overall simulation time and allowed for the large turbulent structures to develop beforehand. The WALE sub-grid model was used to model the small-scale turbulence. The solution time was $0.7s$ which is approximately 7 flow passes for the domain. Mean field monitors were setup for flow variables such as velocity (components) and pressure. Time averaging of instantaneous values were performed between 0.3 and 0.7 s, this gives time for the simulation to iron out the initial flow discrepancies. A time step of $2 \times 10^{-5} s$ was used, this can be shown as an adequate time resolution by monitoring the *Convective Courant* number at points in the domain (see Appendix A). The coupled implicit solver was used with 8 inner iterations per time step. Again, this was deemed adequate as numerous pressure and velocity point monitors showed stabilizing behaviour for each time step (see Appendix A). Second order temporal scheme is used for its superior accuracy.

3.3.4 Divergence issues and remediation

Initial attempts at the LES were unsuccessful due to divergence problems which originated from cells near the pressure outlet inside the engine bay. This was possibly due to the simulation being over-constrained by the pressure values mapped to the outlet. To remedy this, the domain was extended using a $1m$ long box section. This allowed the flow fluctuations to even out over the distance and greatly improved the LES stability. An in-place contact interface between the test domain and the extension allows this to happen. The rear side of the extension is a pressure outlet set to what would be the average pressure of the outlet that it replaces. The extension

region was meshed using the polyhedral mesher using a base size of 10 mm. The region has around 17000 cells.

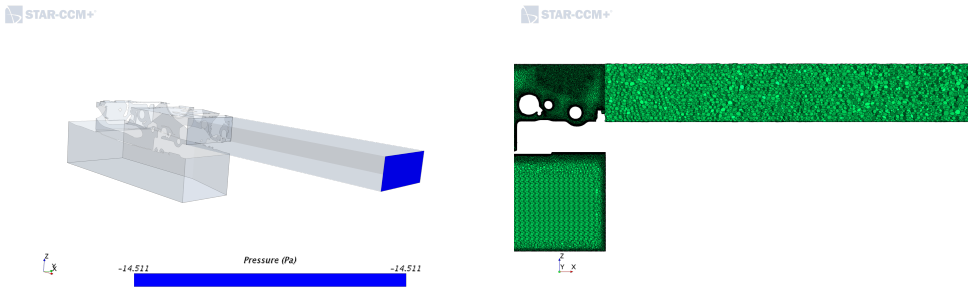

(a) Extension position and pressure outlet

(b) Mesh for the extension

Figure 3.15: Extension added to the test domain.

Additionally, the time step was set to $1 \times 10^{-5}s$ for the first $0.2s$ along with the 1^{st} order temporal scheme to ensure stability. This was switched back to the original settings for the rest of the solution time.

3.4 Steady state method for under-body ducts

The main objective of this study was to develop a steady state method (using RANS) for under-body ducts and to evaluate the usability of such a method in a vehicle thermal simulation. The test domain used in LES, including the domain extension, is used here. This allows for an exact comparison between the LES and RANS results and the quality of the RANS method can be properly assessed.

3.4.1 Meshing, boundary conditions and simulation setup

The meshing strategy developed in the preliminary study was adopted for the test domain. A trimmed mesh cell was used with volumetric refinement performed near the ducts using cylindrical refinement zones (configuration 2, see Table 3.1). The size and location of these cylinders are relative to the individual duct sizes. These relative proportions were kept identical to what was used in the preliminary study.

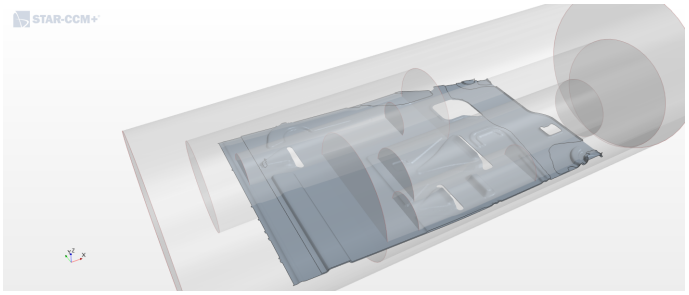

Figure 3.16: Refinement zones, relative sizes and locations

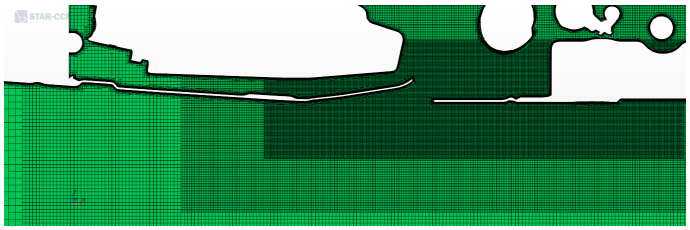

Figure 3.17: Mesh for the RANS method, sectional view, Duct 2 mid-plane

Mesh	Base size (mm)
11M	16
20M	10
30M	8

Table 3.4: Base sizes for the RANS model, under-body ducts

Boundary layers are resolved using prism cells. The total height of the prism layers is around 5 mm, the same as that used in the LES, but with a growth rate of 1.30 instead of 1.10. A total of 18 layers was needed for a y^+ of 1 near the walls. Turbulence was modelled using $k - \omega$ SST and the simulation setup was identical to that in the preliminary study. Boundary conditions used were identical to the LES, including the extension box. To assess convergence, the mass flow through the ducts were monitored. Additionally, the average wall shear stress on the target component for Duct 1 was monitored.

4

Results and Discussion

4.1 Results of the preliminary study

The simulations were run for a number of velocity ratios. Several different meshes were generated by changing the base cell size, allowing for a grid convergence study. Figure 4.1 shows some of the simulation results.

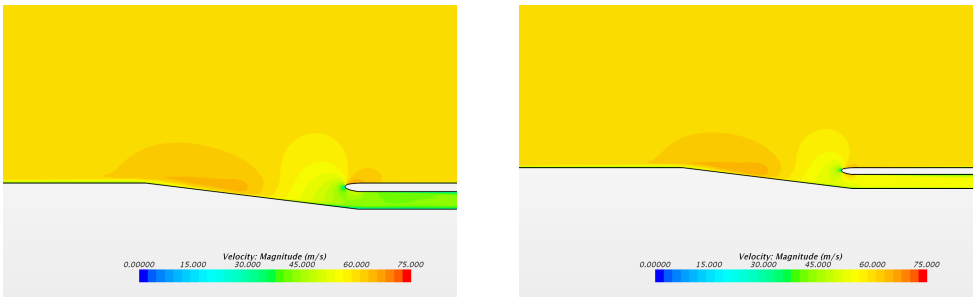

(a) $\nu = 0.6$ **(b)** $\nu = 0.8$

Figure 4.1: Velocity magnitude, duct mid-plane. Mesh size $\approx$ 7.2 million cells

It was found that the CFD setup was able to capture the vortex sheet formation as shown in Figures 4.2 and 4.3

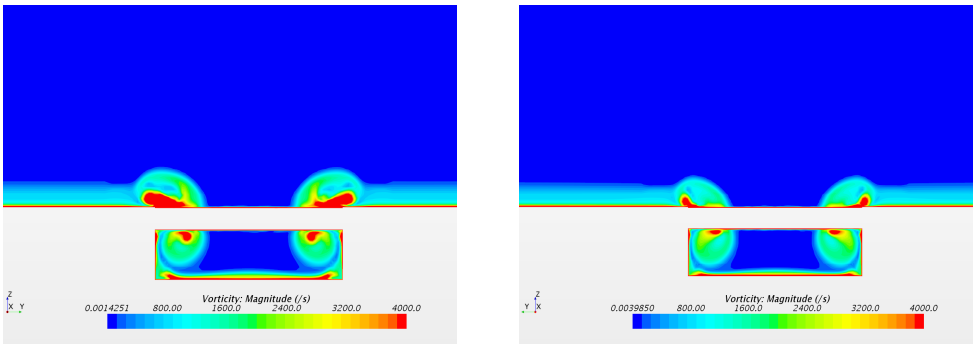

(a) $\nu = 0.6$ **(b)** $\nu = 0.8$

Figure 4.2: Vorticity magnitude, duct entrance plane. Mesh size $\approx$ 7.2 million cells

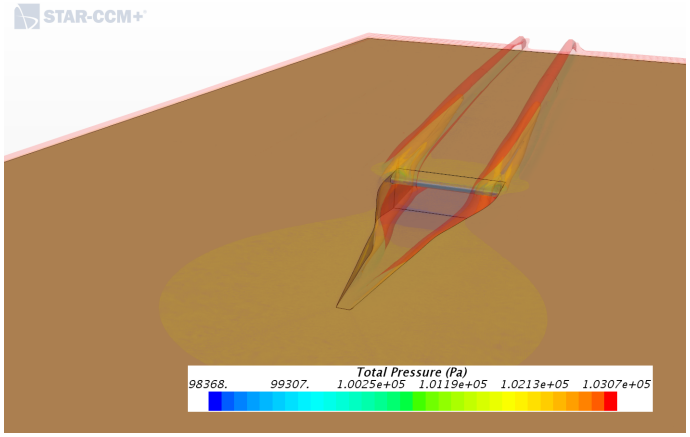

Figure 4.3: Total pressure isosurfaces showing the formation of vortex sheets along the edges of the divergent walls, $\nu = 0.6$

The simulation results are checked against experimental data. The results for ram recovery ratio (see 2.2.2) for different velocity ratios are shown in Figure 4.4. It was observed that the steady state CFD method employed produces agreeable results for velocity ratios between 0.6 and 1.0.

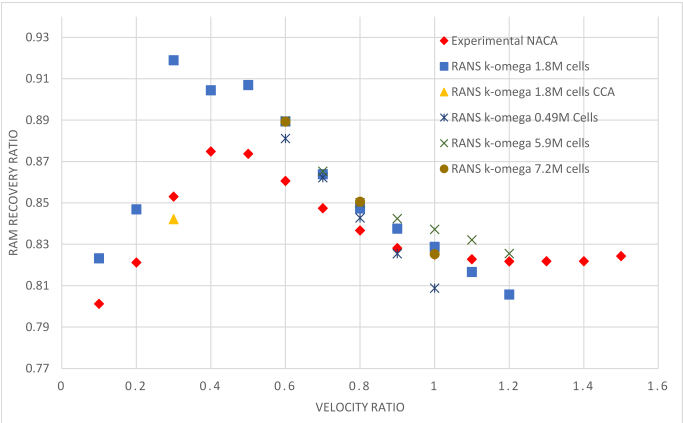

Figure 4.4: Ram recovery ratio results. Experimental data from reference [1]

It does not perform as well for the "transition" region ($0.3 < \nu < 0.5$), over which the ram ratio recovery shows a decreasing trend. Additionally, over these operating points the solver showed poorer convergence with *transient effects* appearing in the convergence monitors and residuals, notably at $\nu = 0.3$. Different results were obtained using the *Continuity Convergence Accelerator* expert driver (marked as CCA in the figure). A plausible explanation for this is that the flow physics over the transition point ($\nu = 0.4$) is too complex for a steady state solution. Hence, the results obtained using the convergence accelerator may not be accurate.
A number of mesh sizes ranging from 0.5 to 7.2 million cells are tested and grid convergence can be observed for the "middle" region ($0.6 < \nu < 1.0$). Pressure coefficient values (C_p, see 2.2.3) are calculated along the floor centerline of the NACA duct using a line probe. This non dimensional parameter is used to validate the flow behaviour near the surface of the duct (Figure 4.5). A C_p value of zero

indicates that the pressure is the same as the free stream pressure. It can attain a maximum value of 1, which indicates stagnation pressure.

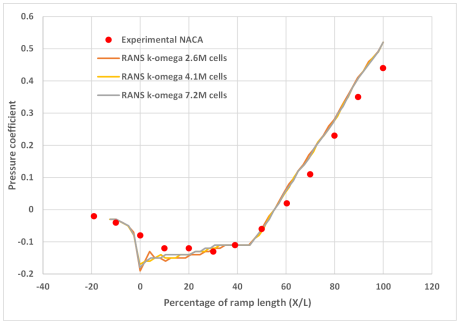

(a) $\nu = 0.6$

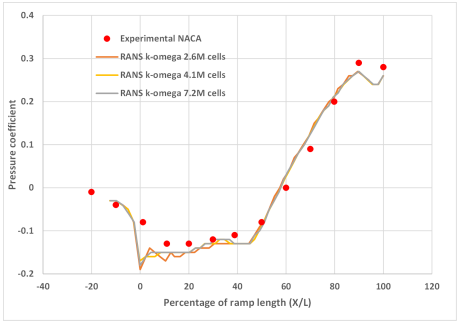

(b) $\nu = 0.8$

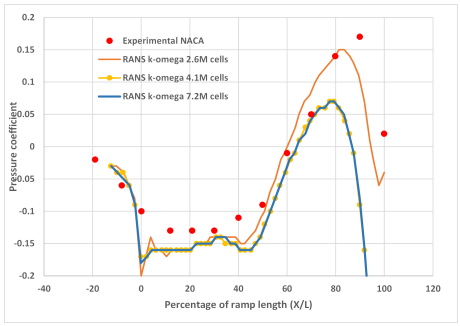

(c) $\nu = 1.0$

Figure 4.5: Pressure coefficient results. Experimental values from reference [1]

There seems to be good agreement with experimental values for two of the operating points that were tested ($\nu = 0.6$ and 0.8). The discrepancy near the tip of the duct ($X/L = 0$) can be explained by Figure 3.6 (a), where, due to the abrupt change in the surface angle, mesh quality is reduced. For $\nu = 1.0$, there is an appreciable deviation near the duct entrance plane, especially for the larger meshes that show similar results. The reason behind deviation is unclear but it's suspected that the complex interaction between the floor boundary layer and vortex sheets is not fully captured in the steady state RANS method.

4.2 Results from the LES

The results from the LES are used as reference for assessing the RANS method. Flow fields (time averaged from 0.3 to 0.7 s) are shown in Figure 4.6

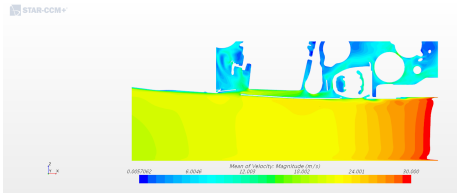

(a) Duct 1 mid-plane

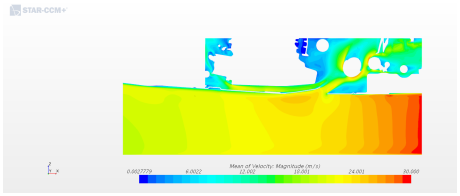

(b) Duct 2 mid-plane

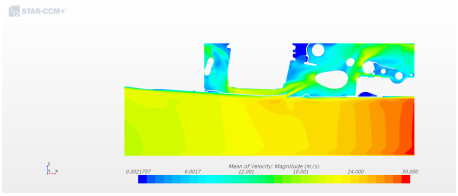

(c) Duct 3 mid-plane

Figure 4.6: Section views of Velocity magnitude (time averaged).

Of the three ducts, Duct 2 is the largest and the one that most resembles the shape of the NACA duct in the preliminary study. The LES is able to show the vortex sheet formation near the duct walls, as show in Figure 3.12

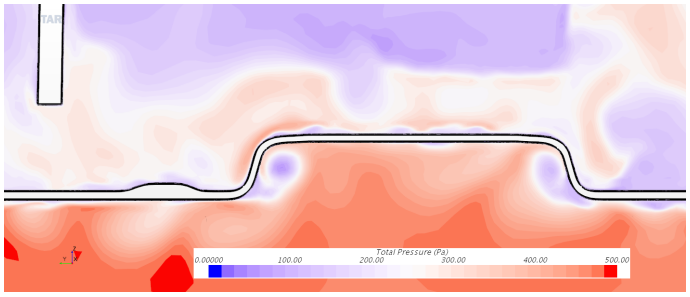

Figure 4.7: Instantaneous total pressure ($t = 0.7s$) for the entrance plane of duct 2 showing formation of vortex sheets.

To check the quality of the LES, scalar fields for modelled turbulent energy ratio (Equation 2.14) is also time averaged. This method is an approximation and is performed only because there is no way to validate the LES results. Figure 4.8 shows that the mesh is able to resolve most of the turbulent kinetic energy ($> 80\%$) near the duct and inside the engine bay, since the modelled turbulence is very small compared to the total turbulent kinetic energy. In the free stream, however, most of the turbulence is being modelled, showing that the mesh is not refined enough, this region is of little interest to this study and so this is acceptable.

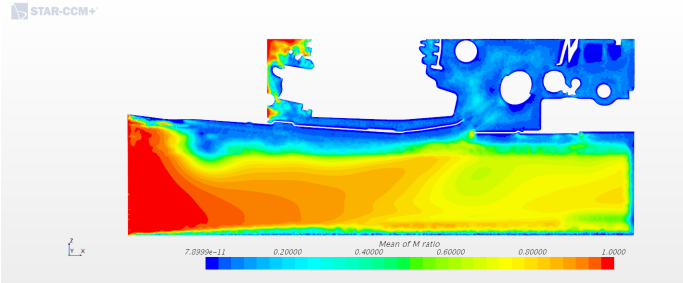

Figure 4.8: Modelled turbulent energy ratio (time averaged;scaled 0-1)

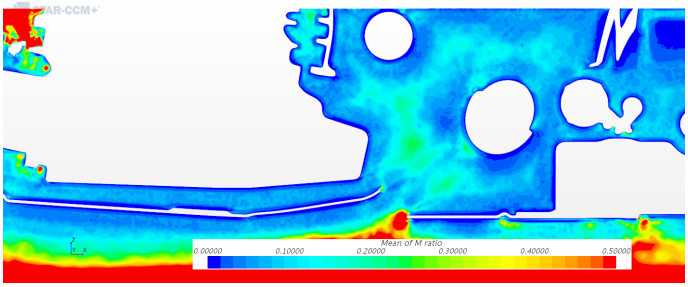

Figure 4.9: Acceptable LES quality in the region of interest (scaled 0-0.5)

4.3 RANS results for under-body ducts

Flow fields for the simulation are shown in Figure 4.10. A visual comparison with Figure 4.6 shows similarity with the time averaged results from the LES.

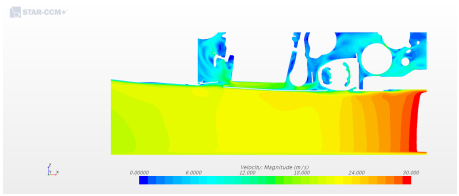

(a) Duct 1 mid-plane

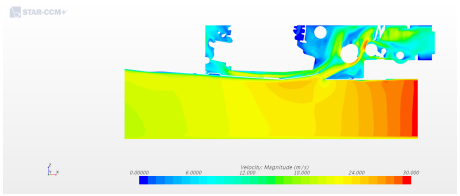

(b) Duct 2 mid-plane

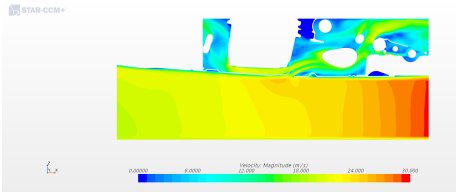

(c) Duct 3 mid-plane

Figure 4.10: Section views of Velocity magnitude

The RANS simulations also capture the vortex sheet formation near the duct walls, as shown in Figure 4.11.

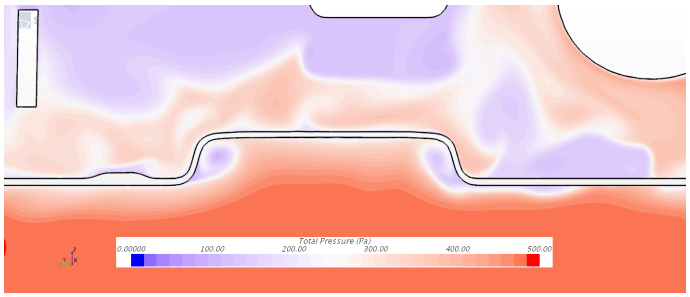

Figure 4.11: Total pressure for entrance plane of Duct 2 showing formation of vortex sheets

4.4 Comparing the LES and RANS results

The accuracy of the RANS method was assessed by comparing the RANS results with the reference case. Three aspects were considered during the assessment.

1. The cooling flow entering the individual ducts.
2. Flow behaviour downstream of the individual ducts.
3. Flow in the rest of the engine bay

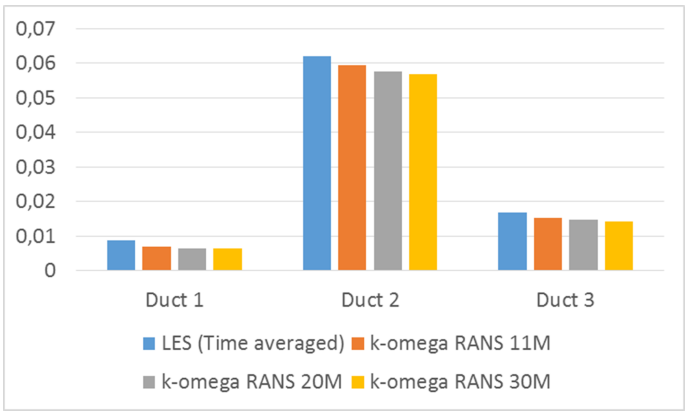

Figure 4.12: Comparison of mass flow rate between time averaged LES and RANS (kg/s)

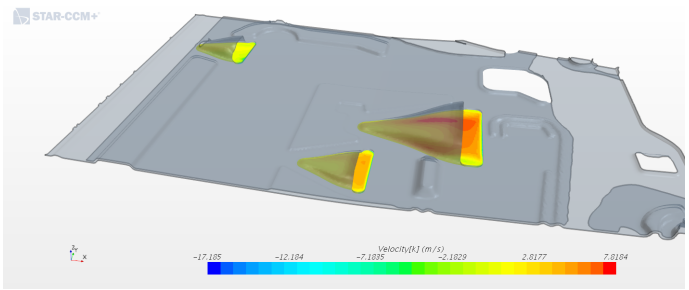

Figure 4.13: Plane sections from which mass flow rates were computed (here they show velocity v_z)

Figure 4.12 shows that the RANS method gives good results for the mass flow through the individual ducts. Even the coarse mesh with 11 million cells captures the inducted flow quite well. Figure 4.14 shows the comparison of pressure coefficient measured along the floor of the individual ducts. The RANS results show good agreement with the reference for Duct 2 and Duct 3. The deviation in the results for Duct 1 can be explained by looking at the flow fields, Figure 4.15. There is flow separation which starts near the tip of the duct. The steady state method is not able to capture the results of this complex flow.

Duct 1 is not a typical NACA duct since the floor angle near the tip is steeper than the recommended 7°, this could be the reason behind the flow separation for this driving case. Mesh refinement seems to improve the results, the fine mesh with 30 million cells seems agree more with the reference but this could easily be a cancellation of errors. These results are consistent with what was found in the preliminary study: A steady state method will not be able to capture complex flow interactions between near the duct surface but should still give good results for the inducted flow rate.

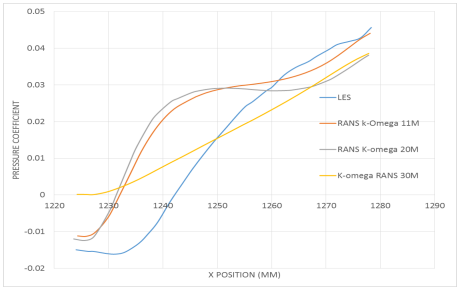

(a) Duct 1 mid-plane

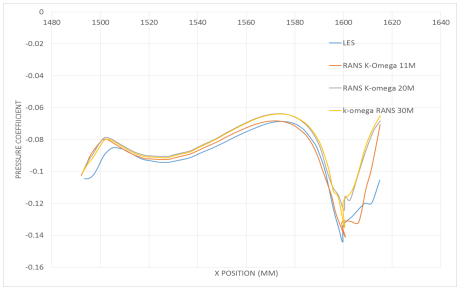

(b) Duct 2 mid-plane

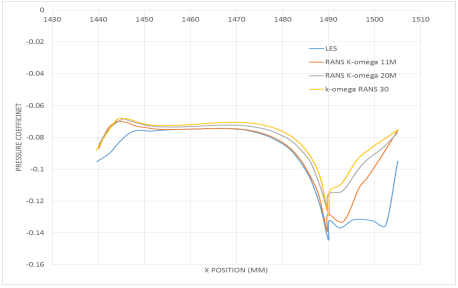

(c) Duct 3 mid-plane

Figure 4.14: Pressure coefficient measured along the floor of the individual ducts

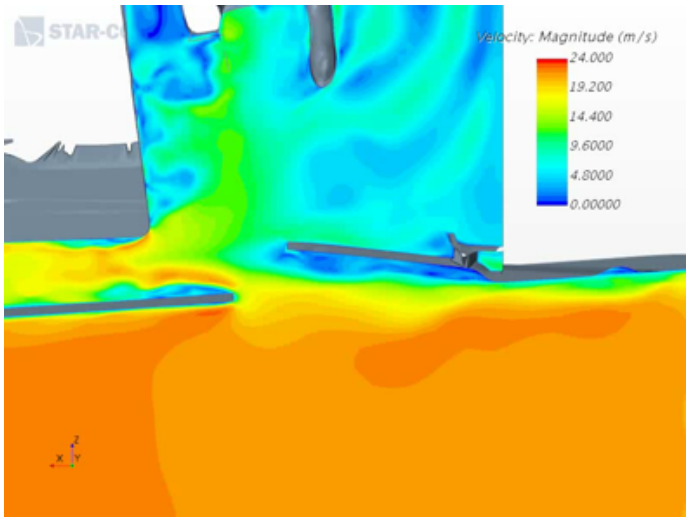

Figure 4.15: Flow separation near Duct 1, LES ($t = 0.3\ s$)

It is important to check the cooling flow path once it enters the engine bay. The wall shear stress is monitored on the target component for Duct 1, a rubber bushing for an engine mounting. This is of interest because, from tests in the wind tunnel, it has been confirmed that the cooling flow for Duct 1 reaches its target.[1]

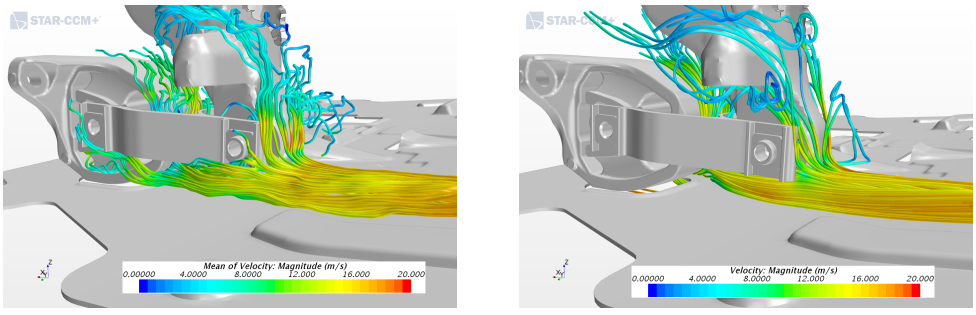

(a) LES, $t = 0.7\ s$ **(b)** RANS

Figure 4.16: Streamlines showing the cooling flow from Duct 1 reaching the target

[1] Temperature readings from the wind tunnel tests show that the temperature of this bushing increases by around 10 degrees when Duct 1 is closed-off. This was for a driving case of 70 *kph* ($\approx 20\ m/s$).

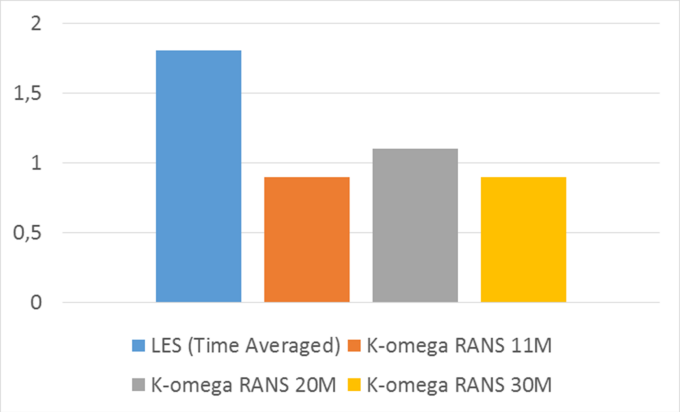

Figure 4.17: Wall shear stress on target bushing for Duct 1 (Pa)

Figure 4.17 shows that the RANS under-estimates the wall shear stress on this component ($\approx 50\%$). This indicates that the cooling flow hitting the target is less that what it should be. Either the inducted flow has dissipated before reaching the bushing or the RANS hasn't fully captured the flow in the rest of the engine bay. In order to test if the cooling flow has dispersed faster than it should have, the flow rate was measured through planes downstream of the ducts (Figure 4.18).

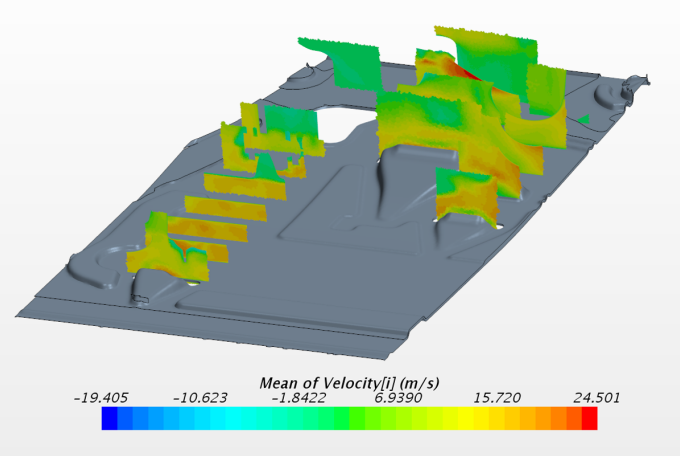

Figure 4.18: Constrained plane sections used to measure flow rate downstream of the ducts.

Figure 4.19 shows that the flow rates downstream of the ducts seem to agree well with the LES reference. It could be argued from this that the cooling flow hasn't dissipated a lot downstream and hence the error in the wall shear stress must originate from the flow elsewhere in the engine bay.

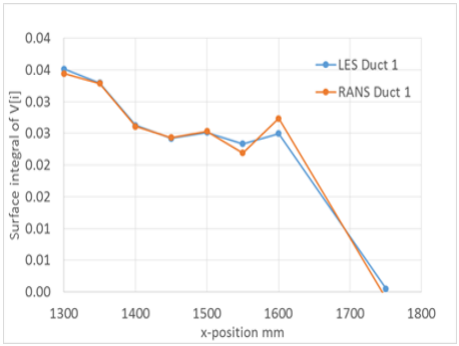

(a) Duct 1

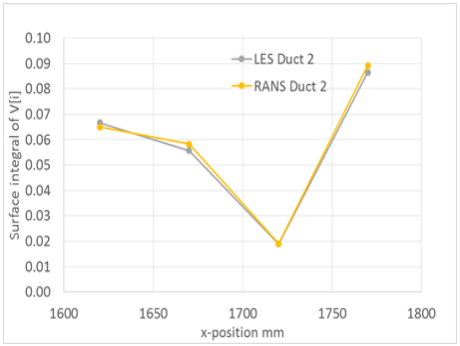

(b) Duct 2

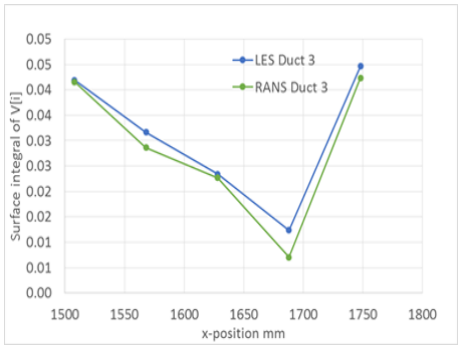

(c) Duct 3

Figure 4.19: Surface integral of velocity v_x measured on the constrained planes. (m^3/s)

Using *data mappers* in STAR-CCM+, the difference between the flow fields between the two simulations can be visualized. Figure 4.20 was obtained by first subtracting the RANS velocity field from the time averaged LES and then generating iso-surfaces of this velocity difference. The velocity differences between 5 and 15 m/s are visualized here.

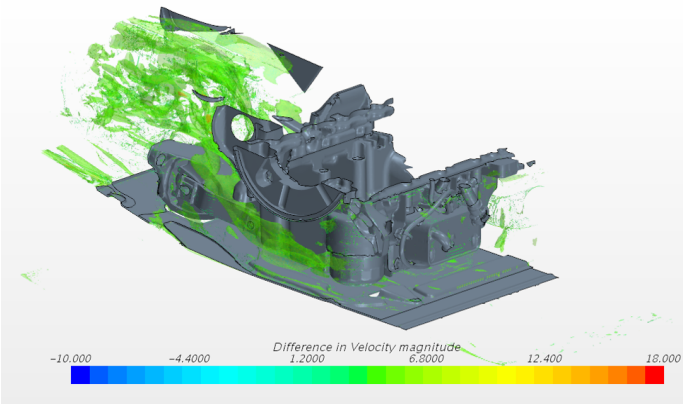

Figure 4.20: Iso-surface showing the difference between the LES and RANS velocity. Picture contains parts of the engine inside the test domain, the engine under shield and the target bushing for Duct 1

The figure above shows clearly that even though the RANS captures the duct flow rather well, there are regions inside the engine bay where the flow is simply too complex for a steady state solution. For example, consider the flow around the cylindrical oil filter (Figure 4.21). The LES shows that the cooling flow from the fan (lies outside the test domain, left of the figure) moves through the space between the engine and the oil filter. The flow then separates and reattaches to the side of the engine and then proceeds to impact the target bushing for Duct 1. This is not captured in the RANS solution and was initially thought to be a contributor to the erroneous wall shear stress results.

Local mesh refinement was performed to capture the flow reattachment, although this seemed to improve the flow field, there was negligible improvement in the wall shear stress results (Figure 4.23). The LES was initialized from a converged RANS solution using an identical polyhedral mesh. The results for this RANS solution shows an error of $\approx 20\%$ for the wall shear stress (Figure 4.23). This clearly shows that the error in the results is a due to the limitations of the steady state model and not due to poor mesh quality.

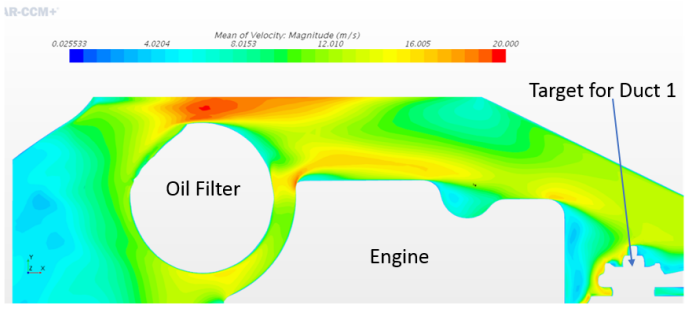

(a) LES, time averaged

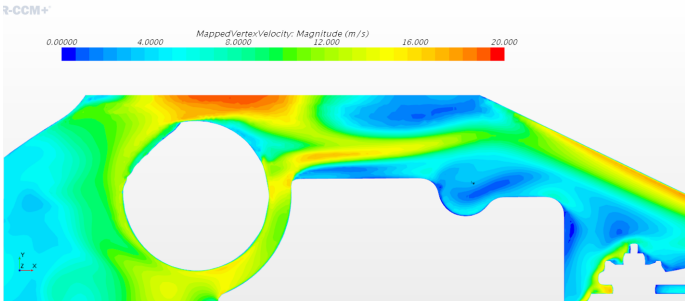

(b) RANS

Figure 4.21: Velocity magnitude near the oil filter. The plane section lies about 15cm above Duct 1

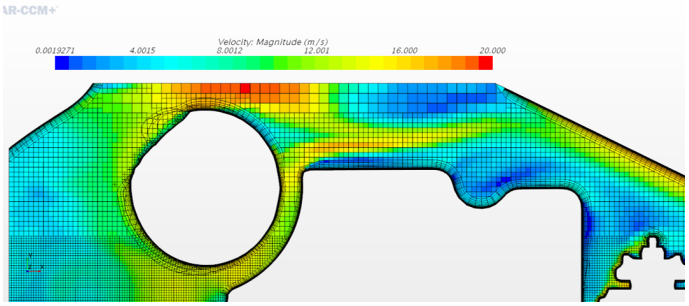

(a) Without local mesh refinement

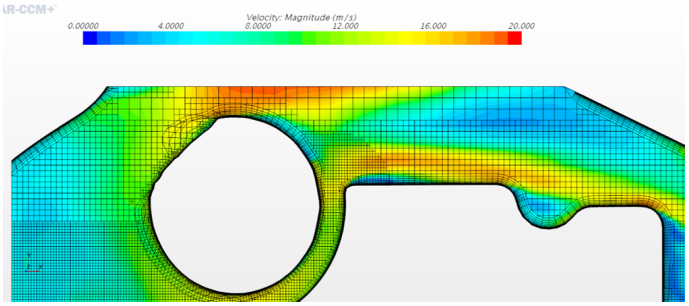

(b) Local mesh refinement around the separation point

Figure 4.22: Local mesh refinement performed for the RANS method shows improved results

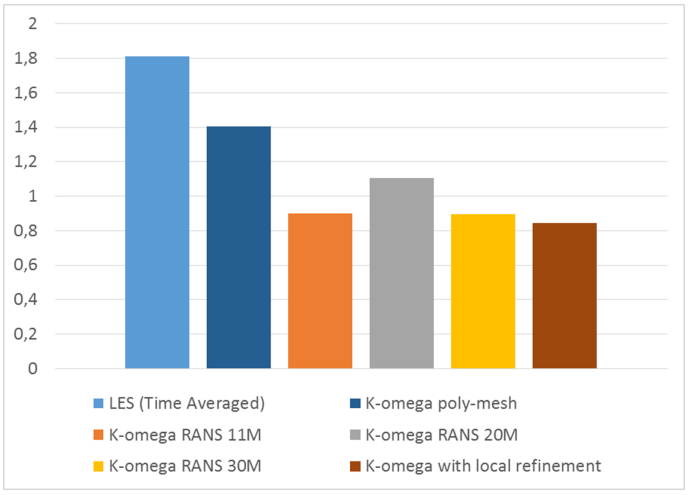

Figure 4.23: Wall shear stress; Results of the mesh refinement and for the polyhedral mesh (Pa)

5

Conclusion

5.1 Evaluation of the RANS method for under-body ducts

The results discussed above show that a steady state method using a carefully designed mesh and a suitable turbulence model should be able to capture the cooling flow through the under-body ducts. In the context of vehicle thermal simulation, however, it should be used with caution as flow in the engine bay is too complex for a steady state model. It's impractical to perform mesh refinement, as shown in Figure 4.22, for all the regions where the RANS method is suspected to encounter problems. As the RANS method is not accurate enough to replicate the LES results, it is recommended to not integrate this into a "full-car" simulation until further investigation has been made. The errors in the engine bay could affect the cooling flow to such and extent such as to produce erroneous results in the thermal simulation.

However, in some simple cases it could probably give satisfactory results. Since mass flows and down stream flow rates are relatively accurate, its use can be justified for larger ducts when the target components are nearby.

5.2 Recommendations and scope for future work

We now know that a steady state method has its limitations when trying to model cooling flows inside the engine bay. However, if such a method is to be used in the design phase (where the sizes and locations of the NACA ducts are decided) it's recommended here to perform the simulations in a reduced domain (like the test domain used in this study) as opposed simulating the whole car. A full car simulation could be used to provide realistic boundary conditions. It's also seen that a polyhedral mesh is better able to cope with the complex flow fields involved.

It would be interesting to investigate if a co-simulation between the reduced domain and the full car domain is possible. Temperature information about the target components can be exchanged between the two domains, indicating the cooling performances of these ducts. Highly accurate results can be obtained by using LES but at a high computational cost. An unsteady RANS (URANS) method should be able to deliver acceptable results at a fraction of the cost, this is worth investigating.

5.3 Summary

The objective of this thesis was to produce a steady state CFD method to model cooling flows through under-body NACA ducts used in cars. A preliminary study on a generic NACA duct geometry provided useful information for this purpose. It was found that a combination of volumetric mesh refinement near the duct surface and a suitable turbulence model can give accurate results for the inducted mass flow as well as the flow downstream of the ducts. However, the steady state method was unable to capture the complex flow phenomenon inside the engine bay and because of this, it was not deemed accurate enough for use in a "full-car" simulation. The results indicate that it might be suitable for special cases where the duct and target component are in close proximity, provided that the simulations be carried out in a reduced domain and use a polyhedral mesh to cope with the complex flow phenomena.

Bibliography

[1] Frick CW *et al.* (1945), *An experimental investigation of NACA submerged-duct inlets* , NACA-MR-A5E23, Research Memorandum

[2] Nicolas J Pignier *et al.* (2016), "Aerodynamic and aeroacoustic analyses of a submerged inlet in a low-Mach-number flow", *Computers and fluids* pages 15-31

[3] Alwin H Sacks and John R Spreiter (1951), *Theoretical investigation of submerged inlets at low speeds*, NACA-TN-2323, Technical note

[4] Jenny C holt and Kevin P Garry (2013), "The impact of inlet flow conditions on the aerodynamic performance of a NACA submerged intake for ground vehicle application", *Journal of automobile engineering*

[5] *STAR-CCM+ user guide v12.02*

[6] Dan Steen, "How to control numerical dissipation of your solution", *STAR-CCM+ documentation*, [Online], Available : `https://thesteveportal.plm.automation.siemens.com/articles/en_US/FAQ/How-to-control-numerical-dissipation-of-your-solution`

[7] Frank M White, *Fluid Mechanics*, 7th edition

[8] John F Wendt, *Computational Fluid Dynamics: An introduction*, 3rd edition, von Karman institute, Springer

[9] Lars Davidson (2017), *Fluid Mechanics, turbulent flow and turbulence modelling*, Lecture Notes

A

Appendix A

A.1 Design of the generic NACA duct for the preliminary study

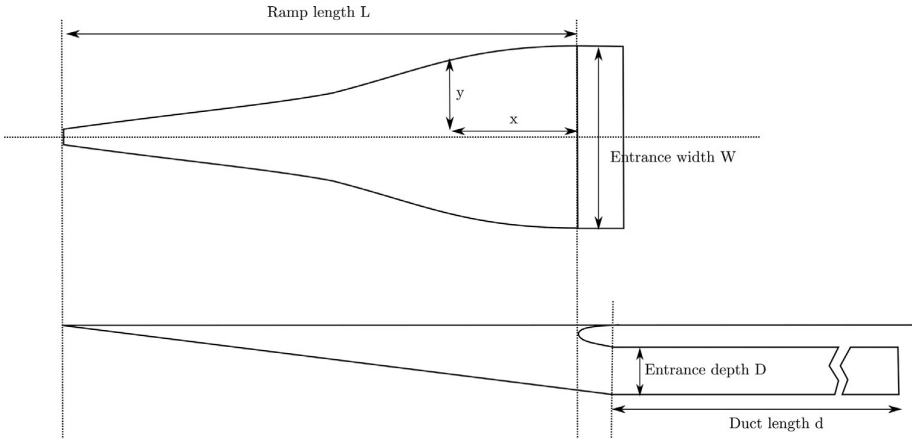

Figure A.1: Generic NACA duct, top view. Figure from reference [2]

D	L	l	d	W
50.59mm	11.31D	0.75D	29.53D	4.00D

Table A.1: Main dimensions. From reference [2]

x/l	y/l
0.0	0.500
0.1	0.497
0.2	0.457
0.3	0.382
0.4	0.307
0.5	0.233
0.6	0.195
0.7	0.157
0.8	0.118
0.9	0.080
1.0	0.042

Table A.2: Divergent wall ordinates. From reference [2]

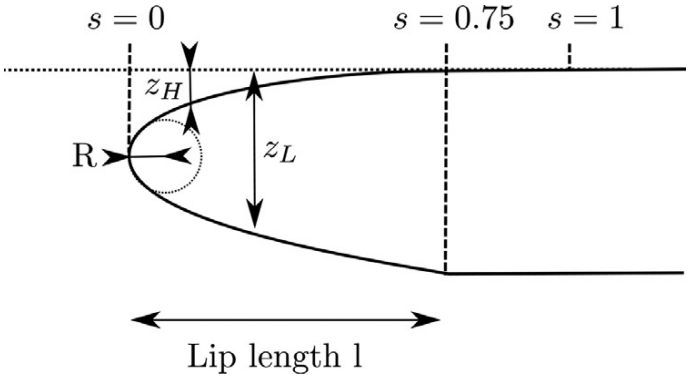

Figure A.2: Generic NACA duct, Lip profile. Figure from reference [2]

s/D	Z_H/D	Z_L/D
0	0.197	0.197
0.125	0.087	0.325
0.250	0.056	0.375
0.375	0.036	0.412
0.500	0.021	0.440
0.625	0.012	0.462
0.750	0.006	0.481
0.875	0.002	-
1.000	0.000	-

Table A.3: Lip ordinates. From reference [2]

A.2 Monitoring the LES

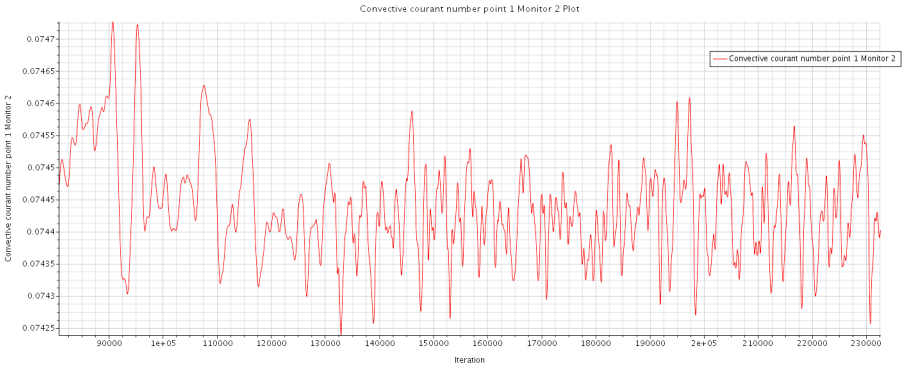

(a) Point in the free stream

(b) Interior points

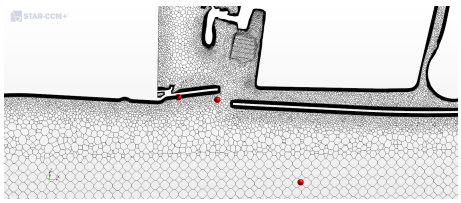

(c) Points monitored

Figure A.3: Monitoring the convective Courant number

From the figure above we see that the Courant number is less than unity even for points where the mesh is extremely fine (sub-figure b). This shows that the time step is adequately small.

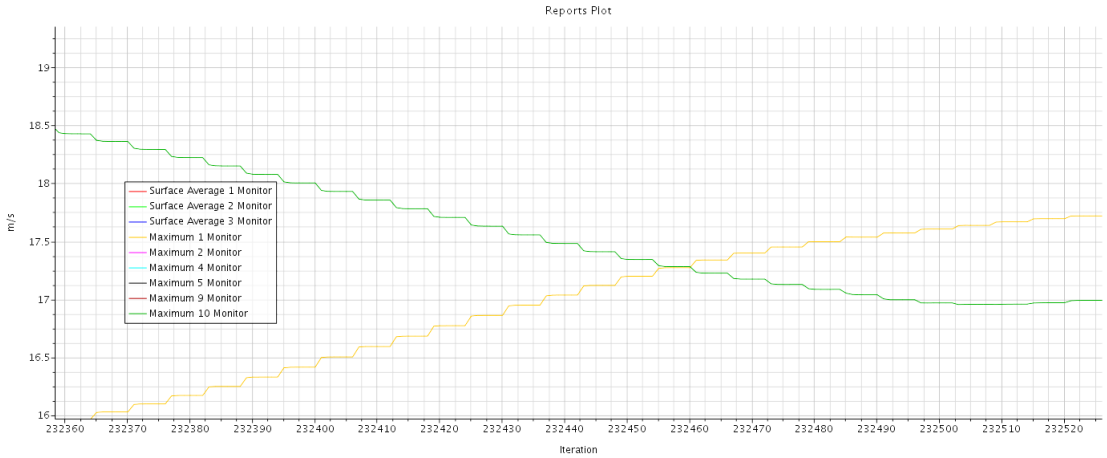

Figure A.4: Stabilizing behavior with each inner iteration for the implicit solver